Text

Analysis of the tide on the Hooghly River; Calibration and alteration of a model computing the vertical distribution of the suspended sediment under non-permanent flow conditions

June 1992

J. de Vletter

TU Delft
Delft University of Technology

Faculty of Civil Engineering
Hydraulic and Geotechnical Engineering Division
Hydraulic Engineering Group

Foreword

In the course of my graduation project I received help from numerous people, whose support has alleviated my efforts. First, I would like to thank my graduation supervisors: Prof.ir.K. d'Angremond, ir.F.van Roode and ir.E.Allersma.

Secondly, I would like to express my gratitude to the people at Hydronamic and Boskalis, who helped me in countless ways with suggestions during my research and with the composition of my report.

Thirdly, I am indebted to my nephew, Peter Willems, for converting my Denglish into English.

In addition, I would like to say thank you to Jan Stinenbosch, my trustworthy chauffeur, who saved me from getting up even earlier.

Last but not least, I would very much like to thank Thijs Schumacher who has given me valuable support during the initial stages of my project and has shown me around at Boskalis.

Delft, 23 June 1992

Joan de Vletter

Contents

Chapter 3 Harmonic analysis of tides

Chapter 4 Theory of the vertical sediment transport over the vertical

Chapter 5 The programme in operation

Appendices

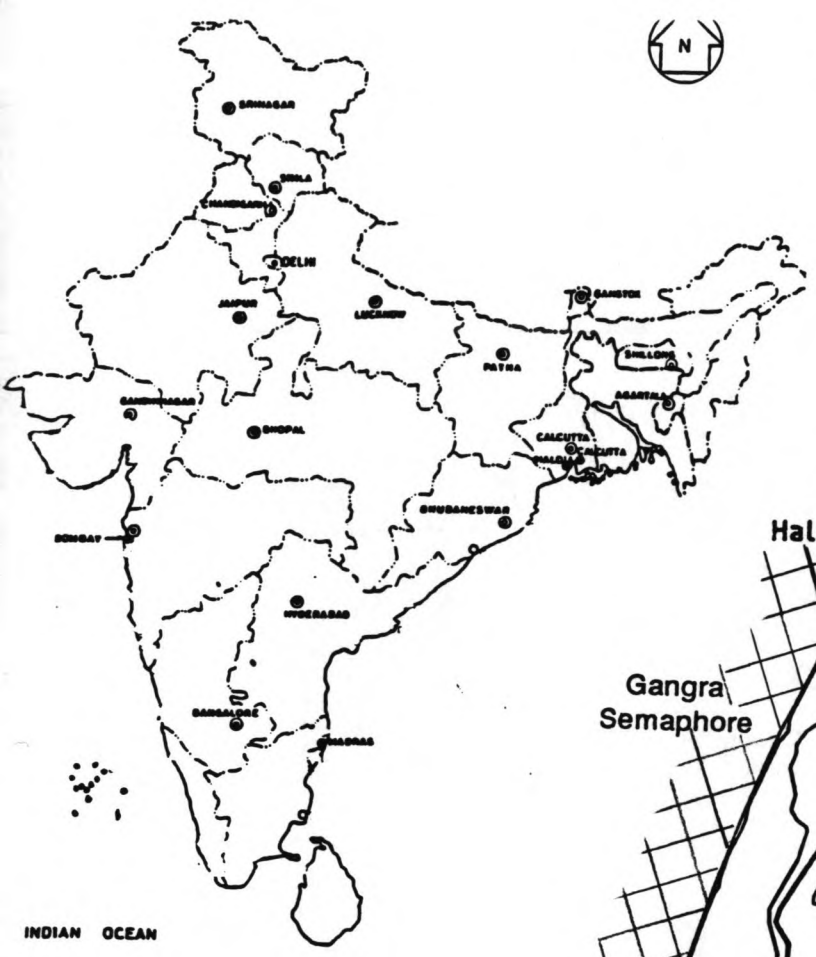

Figure 1

Figure 2

Introduction

The Hooghly river is situated in West Bengal, a Northeastern state of India. The capital of West Bengal is Calcutta. (See ***figure 1***). The discharge from all the eastern and western tributaries, and from the direct head from the Ganga, flows into the Bay of Bengal through the Hooghly estuary. The Hooghly delta is part of the Indo-Gangetic delta.
The harbour of Haldia is situated about 95 kilometres upstream in the estuary. Haldia harbour functions as satellite harbour to Calcutta; mainly coal and oil is transferred here. Many ships need to sail past Haldia to Calcutta and vice versa. The estuary of the Hooghly consists of a number of channels and bars, which can be divided into a flood system and an ebb system as a result of tidal influences in the Bay of Bengal and upland flow. A huge amount of sediment is transported through this system.

Description of the situation

Haldia Harbour can be reached from the Bay of Bengal through Gasper channel, Sagar roads, Jellingham channel and Haldia channel. The latter is part of a flood flow system. On this route, ships need to cross four bars, Gasper, Middleton, Auckland and Jellingham Bar.
Because the performed dredging activities to maintain the draught were not completely satisfactory, only small ships or partly unloaded ships are able to pass the bars. Vessels may also be restricted to certain tidal windows. The target draught of Haldia channel was set on 10.67 m. In 1980 9.14 m vessels were able to enter the harbour for 10 days only. The Calcutta Port Trust was appointed by the Indian Government to take care of this problem.

Description of the problem

Vessels heading for Calcutta, can follow two routes (see ***figure 2***):

1. Sailing through Gasper channel, Sagar roads, Jellingham channel to Haldia channel, then crossing Balari Bar to Kulpi Roads, and further upriver.
2. Passing Gasper channel, Sagar roads, through Bedford channel via Rangafalla channel to Kulpi Roads.

Upstream Kulpi roads, depth is sufficient, but many ships cannot get across shallow flats in the estuary. A tidal bore is found if the tide difference is more than 4 m.
Route 2 is most often used, due to the fact that Balari Bar is almost completely shoaled. This means that ships need to make a detour, which is uneconomical.

As the accretion progresses, the authorities are afraid of the Haldia channel shoaling completely. In that case, Haldia Harbour will be put out of use. As it happens, Rangafalla channel is predominantly an ebb channel, in which flows are stronger and therefore, shoaling occurs less.

Studies have shown that deepening Balari Bar, following the flow lines, is essential for the improvement of access to Haldia, especially for Jellingham Bar. The optimal position of the future channel was determined after experimenting with a physical model.
Two things were recommended to improve the flow conditions: the building of a guidewall north and south of Nayachara Island and dredging of the channel. The construction of the northern guidewall has almost been completed.

Since intervention in the batthymetry of the estuary after the construction of the channel will provoke alterations in the flow conditions, the amount of sediment transport will change. This influences the erosion or accretion, causing the batthymetry to change again until a new state of equilibrium is reached.
During the dredging of the channel, the transection is locally enlarged, resulting in locally decreasing velocities, particularly if the channel is not completely dredged for the total distance. In that case there is no continuing flow in the deepened part of the channel yet. This leads to increased sedimentation, which has to be removed by maintenance dredging.
In order to predict the amount of erosion and accretion in future (during or after the construction of the channel), one needs to study the hydraulic circumstances and properties of the local sedimentation system.

For this purpose, a sediment transport model can be used in order to predict the amount of sediment, transported through a certain area. The sediment transport is determined via an assumed relation between the velocity and the sediment transport. The amount of accretion or erosion can be determined by establishing the nett amount of sediment transported into, respectively out of, a defined section.

The flow velocity, needed as input for the sediment transport model is usually derived from a flow model. A flow model predicts flow velocities and instantaneous water depths in an area, out of known tidal movement at the boundaries of the area and the batthymetry of the area.

In order to obtain data, a measuring campaign has to be carried out. This data is required as input of the models or for calibration of the models.

Main purpose of the overall study concerning the Hooghly estuary

The main purpose of the overall study is to predict the amount of erosion and sedimentation during or after construction of a channel across a sandbar, by using a relatively small amount of measuring results, to be put in an elementary, one dimensional computer programme.
Using this model should result in an acceptable estimation of the amount of dredging material, obtained during construction and maintenance of the channel.

Goals achieved within this study

In the framework of the overall study, the following actions were undertaken:

-1 A measuring campaign was performed, collecting data
-2 The obtained data has been processed and discussed
-3 A study was made of the tidal movement, which is needed as boundary condition
-4 Further on, a model predicting the distribution of the sediment over the vertical was studied in order to make a start for the sediment transport model for the area
-5 The model was calibrated using the results of the measuring campaign and was altered in a few ways in order to improve the simulation of the data that has been obtained

This model can later on be implemented into a sediment transport model, which can be linked to the flow model, but this has not been achieved yet.

Preconditions

-1 The models should calculate with acceptable accuracy.
-2 The amount of data, required for a reasonable prediction, should be economically acceptable to purchase.
-3 Generally, the sediment transport is a function of the velocity, raised to the power 4 to 5. Thus an error in the calculation of the velocity results in an exponentially increased error of the sediment transport. Therefore, the flow model should calculate more accurate than the sediment transport model.

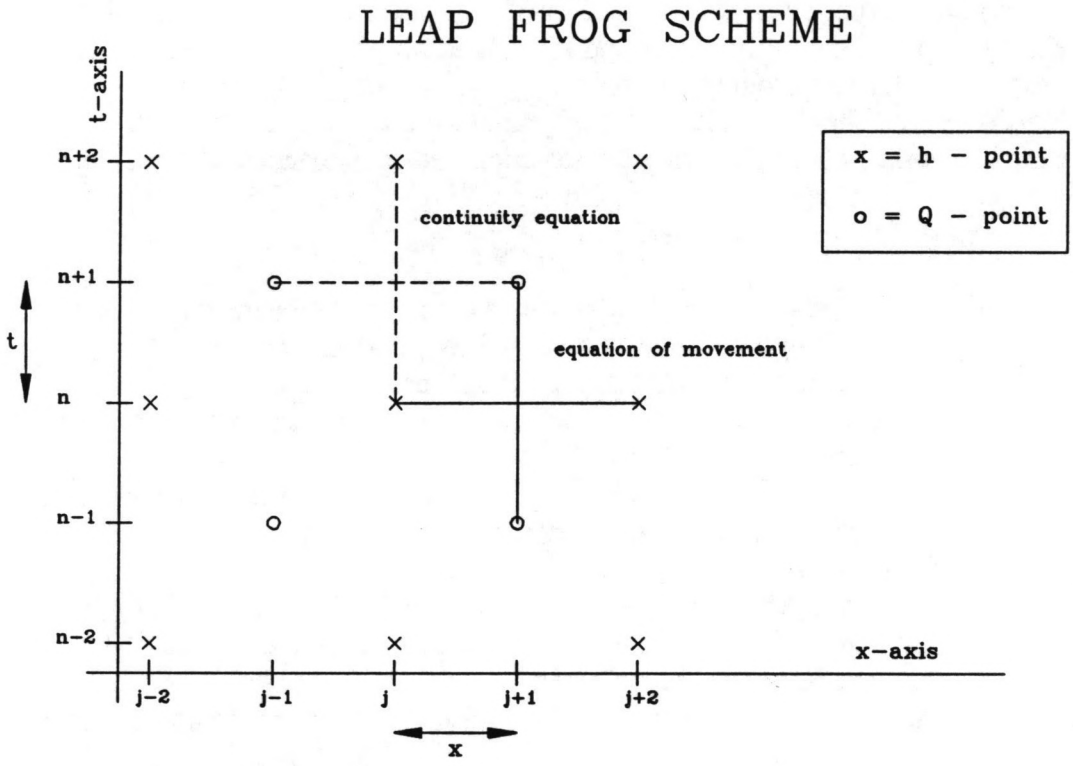
LEAP FROG SCHEME
t-axis
n+2
n+1
n
n-1
n-2
t
x = h - point
o = Q - point
continuity equation
equation of movement
x-axis
j-2
j-1
j
j+1
j+2
x

Figure 3

Assumptions

-1 After critical study of data, obtained by measuring campaigns, the measuring results are supposed to be correct.
-2 The computer programme that represents the flow model, is supposed to be correct regarding calculation of velocity direction and magnitude.
-3 The influence of short period waves is not taken into account in the model of the distribution of the sediment over the vertical. Short period waves are assumed to have a minor effect on the distribution, because of the high velocities that occur in the estuary, which cause a considerable amount of entrainment of the sediment from the bed.
-4 Density currents caused by fresh and silt water confrontation are assumed not to occur in this area during the period of the measuring campaign. The density measurements point to this assumption (see ***section 2.5***).

Short description of the flow model

The flow model, that was developed by predecessors in this study, is studied with a view to the fact that the sediment transport model is going to be attached to the flow model. Both models should schematize the occurring events with the same accuracy.
The programme of the flow model is based on a leap-frog scheme of depth points (h-points) and discharge points (Q-points), see ***figure 3***.

New values of the water depth at the h-points are calculated via the continuity equation:
$h(n+1,j) = f[h(n-1,j), Q(n,j-1), Q(n,j+1)]$
and discharges at the Q-points result from the equation of movement:
$Q(n+2,j-1) = f[Q(n,j-1), h(n+1,j), h(n+1,j-2)]$.
The depth (distance between bottom and Chart Datum) added to instantaneous tidal height (referred to Chart Datum) gives the water level (h).

The depths and tidal heights are input parameters; the batthymetry is schematized into several strips parallel to the channel axis. These strips are divided into smaller sections of uniform depth.

The programme determines the discharges, from which the mean velocities can be derived. The model is calibrated by comparing the determined velocities with the measured velocities. This programme will be extended by a calculation of the sediment transport. This is usually a function of the velocity.

Chapter 1 Measuring campaign

§ 1.1 Introduction

During the months of March and April 1991, the first measurement campaign took place. Velocities, sediment concentrations and water level registrations were obtained, which gave a good impression of the hydraulic situation during these months.
Once a year, the monsoon hits India. The monsoon causes a raise of the mean water level by the wind shear stress and the raise of the mean river level as a result of the increase of the discharge. Over the Bay of Bengal, south-west wind prevails from the end of April to October. During the other months a lighter north-east wind blows. During the monsoon heavy rainfall occurs. The water is drained off by rivers, thus the river flow increases. This means that both discharge and transection may change in magnitude. The effect on the velocity is not known ($u=Q/A$). A second measuring campaign in the monsoon period was found necessary to get a better idea of the flow conditions during the monsoon.

§ 1.2 Preliminary study

§ 1.2.1 Working method

Sediment transport theories are studied to trace all values, coefficients, etcetera, that are needed for research. Existing computer programmes (DUCHESS and ESTRA) are investigated as well, in order to find out what kind of information is necessary to run such programmes. These necessary values must be obtained during the measuring campaign, which can be done with different instruments.

After an investigation of instruments that could be employed, results of the first measuring campaign were evaluated. A number of instruments had already been purchased in the Netherlands and taken to India to be used during a previous campaign. Obviously, these instruments were employed for this campaign as well. The method of measuring and the resulting outcome were evaluated to try to improve future results. By using tide tables a time schedule was made according to the predicted neap and spring tides.

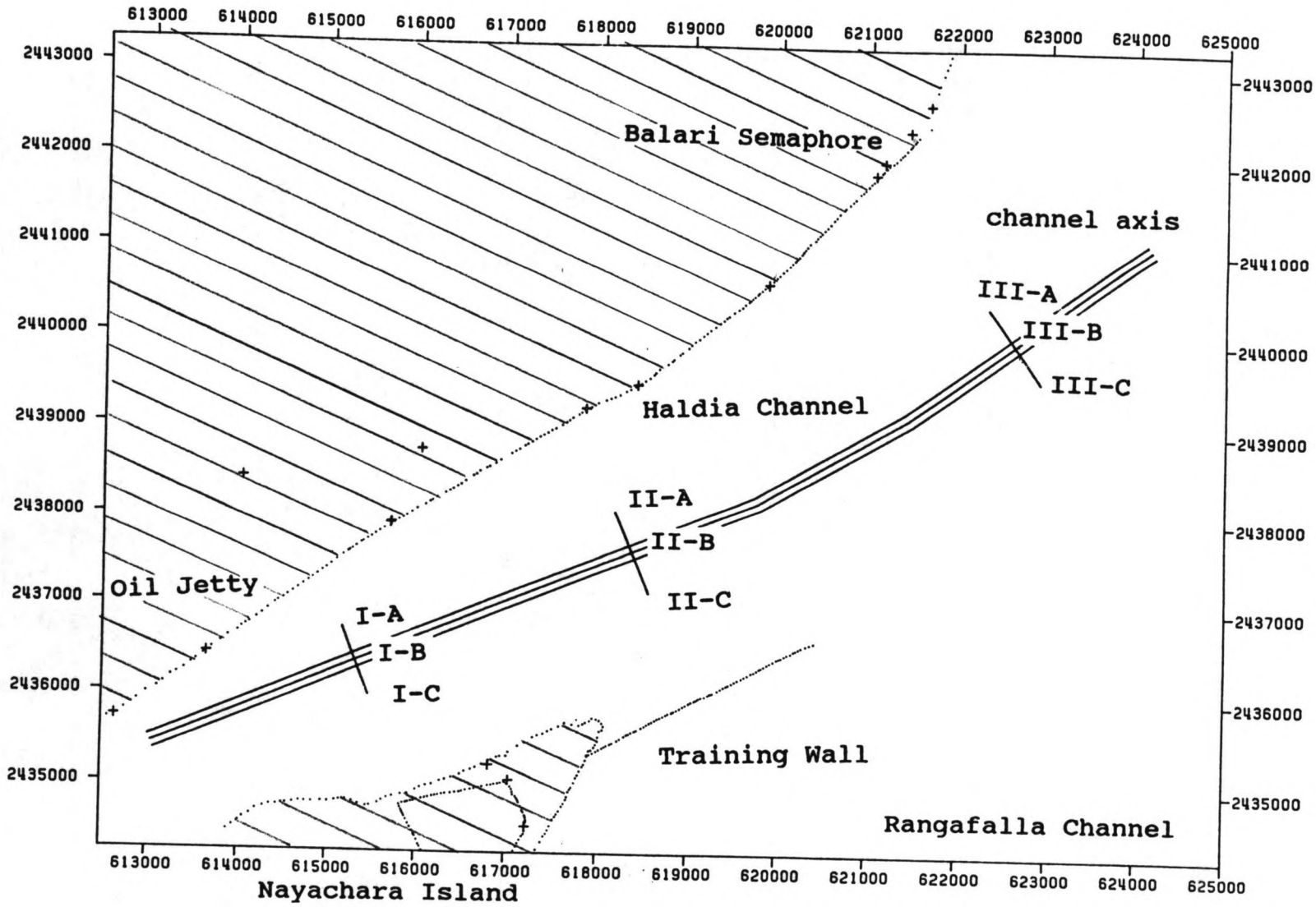
613000
614000
615000
616000
617000
618000
619000
620000
621000
622000
623000
624000
625000
2443000
2442000
2441000
2440000
2439000
2438000
2437000
2436000
2435000
Balari Semaphore
channel axis
III-A
III-B
III-C
Haldia Channel
II-A
II-B
II-C
Oil Jetty
I-A
I-B
I-C
Training Wall
Rangafalla Channel
Nayachara Island

Figure 1.2.3.1

§ 1.2.2 Investigation of information and instruments

The following table displays data needed in order to determine the input and the boundary conditions of the flow and the sedimentation transport models. The table also shows by which means that particular data can be obtained.

Table 1

required data for flow and sediment transport model:	acquired by/ from:
flow velocity and direction	velocity meter
mean water depth in different locations	echosounder
tidal movements at boundaries	water level registrations
mean grain diameter	van Veen grab
concentration profile over depth	Niskin bottle
kinematic viscosity	
mass density of the sediment	
mass density of the water	density float

The kinematic viscosity is a function of the temperature and the salinity. The temperature of the water is measured by the velocity meter. The mass density of the sediment is taken to be 2650 kg/m^3.

An elaborate description of the instruments used for measuring can be found in ***appendix 1.***

§ 1.2.3 Working method during the previous campaign

Along the axis of the proposed channel, three cross sections (I,II,III) were chosen in which the measurements took place. See ***figure 1.2.3.1.***
Cross section I is situated at the beginning of the channel near Haldia; section II lies across Balari Bar, and section III is situated at the end of the channel, which is upstream the division of the Hooghly in Haldia channel and Rangafalla channel. In this way, three different conditions were examined.

In each cross section at three appointed locations (A,B,C) the velocity was measured. The reason for taking three positions is, that the original computer programme schematized Haldia channel as three separate channels, which are linked. In each cross section, the velocity was measured in turns at the three locations for two minutes. At the midpoints water samples were taken during a period of 12 hours. This all took place in two days.

§ 1.2.4 Evaluation and improvements on the previous campaign

The advantage of the working method of the first campaign was that at the same time, measurements took place at several different locations, which is necessary for the computer programme. The draw back of this method is the relatively long time interval between measurements at one location (40 minutes at the midpoint and 80 minutes at the other locations). This is fairly long, considering the rapid change of for instance the water level (which indicates a quick change in the instantaneous velocity).
The method was also largely dependable on the weather, because of the variety of different actions to be taken on the same day.

A different strategy was followed for the second measuring campaign during the monsoon. One location, I-A, was appointed as reference location. During the complete measuring campaign, the velocity is measured in this position. One day was appointed as reference day. On other days, the velocity is measured in other locations as well as in I-A.
Presuming that the difference from the reference day in position I-A, as a result of variations between neap and spring tide, is typical of every other location, data that had been obtained at the other locations on other days are going to be converted to the reference day.
Position I-A was chosen as reference position, because it is close to the jetties and can therefore be easily reached. Moreover, location I-A is deep enough to prevent it from being uncovered.

The flow velocity was measured at the same positions (9) of the three cross sections as during the first campaign. Two new positions were added: Kp 8000 in the middle of the channel-axis near Balari Bar, and a position near the training wall north of Nayachara Island.

On three days water samples were taken every half hour. In each cross section one position is appointed: I-A (on the reference day), II-A and III-B. A bottom sample has been taken every day with a Van Veen grab.

§ 1.3 Planning of the monsoon campaign

The second campaign was meant to take place at the end of the monsoon, when the river is in spate.

Water levels are effected by both the spring-neap variation and the fortnightly influence of the tide. Tide tables show that on the 29th of July the tidal range will reach its maximum. The tidal movement during the measuring campaign is shown in ***figure 2.1, appendix 2.1.***

July the 27th was taken as reference day; two days before the maximum tidal range. For this reason, the velocities will be considerable, but not at their maximum. Therefore, the velocity on this day is thought to be representative for a

whole period of fourteen days. Using this velocity in a sediment transport calculation will result in an average sedimentation transport. On this day both velocity meters were positioned in I-A and measured the velocity at two different depths.

On the days before and after reference day the velocities were measured in the other locations. Locations II-B and II-C are situated in shallow water, thus measurements in these locations must take place around neap tide in order to be assured of sufficient draught.

The planning concerning the measuring campaign was performed, by taking into account the above mentioned details.

§ 1.4 Actual Measuring Campaign

§ 1.4.1 Velocity measurements

Velocity measurements had the highest priority during the campaign. The velocity was registered at one location during approximately 24 hours. The velocity was measured simultaneously at two locations. One of the locations was I-A, the reference location.

§ 1.4.2 Water samples

Introduction

Water samples were taken at three locations, one location in each cross section. Location I-A was chosen, because it is the reference location. Samples were taken in III-B, because its location is situated on the channel axis. Therefore, the samples give information in the area, which is interesting for dredging. The third location, II-A (near Balari Bar), was the deepest location in cross section II, thus it had the smallest chance of being uncovered.

Sampling

Water samples were taken with a Niskin bottle near the bed and water samples at the surface were taken with a bucket.

At location I-A the samples were taken from a fixed position (the pontoon). This was not always easy because of strong flows. Influences of the pontoon on the flow (turbulence), and thus on the sediment concentration, need to be taken into account as well.
The second sampling day took place in III-B. The water samples were taken from the survey boat, drifting near the location. In this way the flow did not bother the Niskin bottle so much.
During the third sampling day, samples were taken in II-A similarly to the second day.

§ 1.4.3 Soil samples

The soil samples were taken with a Van Veen grab, preferably on the same day as the velocity meter registered the flow velocity on that location. In every location (except for I-A), the samples were taken from the drifting survey boat at the time of slack water, in order to minimize flow forces on the instrument.

§ 1.4.4 Transections

The computer programme needs water depths as boundary conditions. Water depths were obtained from echo sounder registrations with simultaneous time registration. After correction for the tide, the actual water depth related to a certain level (here Chart Datum) became known. Mean Sea Level is at Chart Datum +2.82 m.

During the first campaign the surveyors sounded the complete Haldia channel. In the monsoon campaign, the circumstances were more improvisational, thus only the area in which the biggest changes in depth were expected was sounded, which is near Balari Bar. Therefore, the channel axis and area around section II were measured, because these lines gives the best information about the track that needs to be dredged.

§ 1.4.7 Floats

Floats help to define flow lines, which give a lot of useful information about flow magnitude and direction. During the first campaign, floats were set out during flood, thus flood lines were defined. During this campaign it was tried to define ebb stream lines, with specific details on the streamlines near the training wall and the head of Nayachara Island.Some floats in Haldia channel crossed the training wall to Rangafalla channel and one float was trapped in an eddy near Nayachara Island. The operation was repeated several times to optimize the results.

§ 1.4.6 Water level registrations

On several locations at the Hooghly there are CPT stations, where water levels are registered. The locations in the surroundings of Haldia channel were visited to obtain the half hourly registrations and the drawing of the tidal curve of the machine itself. The locations that were visited were:

Gangra Semaphore
Oil Jetty Station
Balari Semaphore
Diamond Harbour Station

The semaphores and Diamond Harbour Station used pressure boxes to measure the water level: the Oil Jetty Station was equipped with a float and the value of the water level at Gangra was obtained by visual reading. At Balari Semaphore, pressure was measured at a distance of about 1 kilometre across the river from the registration office itself.

§ 1.5 Data Handling

Soil samples

Back in Holland, the samples were treated with a wet sieving method: they were dried again and the residue was made to pass the coarser sieves. Afterwards, grain size distribution curves were determined.

Water samples

The reason for taking the samples was to determine the sediment concentration at a certain location at a certain depth. At one location at one time, two samples were taken: one sample at the surface and one sample at about 1.3 m above the bottom.

A certain amount of the water sample (usually 100 ml) is filtrated through a preweighed filter. This filter is dried in the oven and weighed again. Then the concentration can be determined. An elaborate description of the filtration method can be found in ***appendix 1***.

The density of the samples is determined by using a density float. Part of the (shaken) sample is poured in a bamboo tube, the float is put in and read off.

§ 1.6 Conclusions

The time schedule was fairly realistic, although the order of events changed sometimes.

A minor change in the working method was made: the water samples were taken from a drifting ship. Consequently, forces on the instrument were smaller.

Measuring of velocity verticals was neglected, because of the strong forces on the instrument. Salinity data was considered to be unreliable and hence not collected.

Chapter 2 Discussion of data

Introduction

The measuring campaign was performed to purchase data on the area near Haldia on the Hooghly River. These data exist of:

-1 water level registrations
-2 flow velocity measurements
-3 surface and bottom concentration measurements
-4 water density measurements
-5 soil samples
-6 transection depth measurements
-7 float tracks

In the following sections, the collected data will be described and criticized on its accuracy and method of acquisition. The locations, in which the water samples were taken are described extensively, because the data of these locations is used in ***chapter 5***. The data on velocity, that is obtained in the other locations, is examined to get a better overview in the hydraulic system of the area.

The sounding data and flow tracks are not described in this chapter, because this information is not useful in the framework of this report (though the information is quite important to the flow model).

§ 2.1 Water level registrations

The water levels are registered every half hour at the registration stations of the Indian Calcutta Port Trust. This data can be checked with the curve drawn at the drum in the semaphores. The high and low waters are also written down. The data of the Oil Jetty Station is applied for an analysis of the tidal propagation in chapter 3.
Figure 2.1, appendix 2.1, displays the tidal curve during the measuring campaign. Around the first spring tide, the mean water level is set up in consequence of a storm, which shows clearly in the low water levels. The daily inequality is reflected at the top and at the bottom of the signal.
The tidal range and high and low waters during spring and neap tide in the period of the measuring campaign are shown in ***table 2.1***. The measuring campaign took place from 26/07/91 to 12/08/91.

Table 2.1

Oil Jetty	Neap tide [m +CD]	Spring tide [m +CD]
High water	4.5 m +CD	6.5 m +CD
Low water	1.8 m +CD	1 m +CD
Tidal range	2.7 m	5.5 m

§ 2.2 Velocity measurements

Overview

The days on which the velocities were measured are written beneath ***figure 2.1, appendix 2.1***. The measurements in cross section I took place a few days before spring tide. The tidal amplitudes of these days are fairly equal. This also holds for cross section II, although these measurements took place during neap tide. The measurements in locations III-A and III-B succeed each other, but the measurements in location III-C took place near neap tide. ***Table 2.2*** shows the maximum velocities during ebb and flood in the locations of cross section III and in I-A on the same days.

Table 2.2

Location	Sampling date	maximum velocity during ebb [m/s]	maximum velocity during flood [m/s]	maximum velocity during ebb in I–A [m/s]	maximum velocity during flood in I–A [m/s]
III–A	31/07/91	1.8	2	1.4	1.9
III–B	01/08/91	1.6 – 1.75	1.6	1.45	2.1
III–C	04/08/91	1.2 – 1.4	0.8 – 0.9	0.9	1.3

The decrease in velocity in III-C compared to III-A and III-B is similar to the decrease in I-A as a result of the neap-spring variation. ***Table 2.3, appendix 2.2*** shows the maximum velocities during ebb and flood with corresponding depths of the meter, recorded in location I-A. The maximum velocities during ebb and flood with corresponding flow directions and depths of the velocity meter in the other locations are shown in ***table 2.4, appendix 2.2.***

§ 2.2.1 Description of velocity meter output

The velocity meter measures:

-1 the velocity
-2 the direction of the velocity
-3 the depth of the meter below the water surface
-4 the temperature of the water

Every minute, these items are determined and registered on a magnetic card. The graphs show magnitudes of the velocity, that fluctuate around an average velocity. The fluctuations are highest when maximum velocities occur. The ***figures 2.2.1.1 up to 2.2.1.5, appendix 2.1***, showing the data, are composed of four graphs:

-1 Tidal curves from the four registration stations on the measuring day. A phase lag and water level correction need to be applied in order to determine the exact water level in that particular location. However, the curves give an indication of the tidal range in comparison to the neap-spring variation.
-2 The magnitude of the velocity in the flow direction in cm/s.
-3 The angle of the flow direction in degrees with regard to the north.
-4 Depth of the velocity meter in meters under the water surface.

The values mentioned in this section are roughly estimated from the figures with accuracies as shown in ***table 2.5***. These values are meant to indicate certain phenomena and are not applied in calculations. More accurate data can be read in the files from the magnetic card of the velocity meters. This was not necessary for this purpose.

Table 2.5

variable	accuracy
velocity	5 to 10 cm
current direction	5 to 10 ^{0}
depth meter	0.10 m
water level	0.20 to 0.30 m

Table 2.6, appendix 2.2, shows the data that is purchased at the locations, in which the water sampling took place, and at the extra locations: KP8 and TRW, near the training wall. The data exists of:

- high and low water levels at the Oil Jetty station at the same day
- maximum velocities during ebb and flood in the locations as well as in I-A at the same day
- the current direction at the time of maximum velocities

The numbers of the figures, showing the data, are mentioned in ***table 2.6.***

Striking details are discussed below.

Tidal curve

II-A: The amplitude has decreased, compared to location I-A and the mean water level is lower as a consequence of the fortnightly variation, because the measurements took place during neap tide. The same effect occurs on the day of the measurements at TRW.

Velocity

I-A: The maximum magnitude of the velocity is about 2.25 m/s during flood and 1.5 m/s during ebb. This shows, that Haldia channel is predominantly a flood channel, although the current is fairly strong during both ebb and flood.

II-A: The velocity is smaller in II-A than in I-A on the same day. The shape of the curve differs from the curve in I-A: the maximum ebb velocity in II-A is topped off. The velocity near the bar is obviously smaller than that at the sea side of the bar (I-A). Location II-A is situated in a flood channel.

III-B: Both ebb and flood velocities are of the same magnitude contrary to the velocities in I-A on that same day. In location III-B, influences of both Haldia channel and Rangafalla channel are noticeable. Rangafalla channel is an ebb channel, which may explain that the maximum ebb and flood velocities are of the same magnitude.

KP8: The velocities for ebb and flood are almost equal to each other, with maximum values of approximately 1.3 m/s. The asymmetrical form of the curve might be caused by the presence of intertidal flats, which fall dry during ebb, diminishing the cross sectional area, which influences the magnitude of the velocity.

TRW: According to the respective ebb and flood velocities, the training wall lies near an ebb channel. During flood, the velocity increases fast in the beginning up to 0.70 m/s, but next it diminishes down to a constant level of 0.50 m/s.

Current direction

I-A: The average direction of the velocity is about 250^0 during ebb and about 70^0 during flood. These directions along a period of neap and spring tide are likewise.

II-A: The direction of the flow is similar to that in I-A: during ebb it starts at 230^0 and ends at 275^0, with a peak to 350^0 at slack water. When the tide turns, the direction gradually turns via $360^0=0^0$ to 70^0. The direction slowly turns during ebb and is constant during flood. A possible explanation of this turning during ebb could be that when the water level falls, the shallow parts of the estuary are uncovered. This may influence the direction of the current.

Depth of velocity meter

The depth of the velocity meter varies during the tide. The velocity meter tends to drift towards the water surface, when the velocity is high.

II-A: The depth of the current meter is almost constant, except for the uplift during flood.

§ 2.2.2 Variation of the velocity in I-A over the neap-spring period.

The velocities must be known at every location at the same time for calibration of the model. The idea was to measure the velocity in I-A every day and simultaneously in other locations (one location per day). By comparing the velocities at location I-A over the neap spring period, the influence of the neap-spring variation on the velocity can be determined. In this way, the velocities in the other locations can be converted to one day.

The figures, mentioned in this section, can be found in ***appendix 2.1***. ***Figure 2.2.2.1*** shows the maximum flood and ebb velocities over the period of the measuring campaign, measured by a velocity meter that was continuously suspended from the pontoon near position I-A. The depth of the velocity meter differs over this period, which can be seen in ***figure 2.2.2.2***. The difference in depth is either caused by the length of the rope, from which the meter was suspended or by the magnitude of the velocity. The uplifting of the meter is a function of the velocity.

Comparing figures ***2.2.2.1 and 2.2.2.2*** to ***figures 2.2.2.3 and 2.2.2.4***, measurements of the velocities and depths by two velocity meters during the same time period are depicted in ***table 2.7***.

Table 2.7

I–A	velocity	[m/s]	depth of meter [m]	
flood	2.3	2.5	1.5	2
ebb	1.6	2.5	1.9	2.8

Read with an accuracy of 0.10 to 0.20 m, the difference in depth does not have a large impact on the magnitude of the velocity (in the upper layer of the water).

The flood velocities on 27/07/91 are lower at a depth nearer to the surface. This points to the existence of a disturbed flow profile over the depth. This may either be caused by density currents or the influence of the pontoon on the flow. As stated in ***section 2.5***, the presence of salt water in this area is unlikely and the existence of density currents cannot be derived from the limited amount of data available. The influence of the pontoon on the flow is assumed to cause the disturbance of the velocity profile.

The change in depth of the meter in time is merely an indication of the strength of the flow and consequently, of the magnitude of the velocity (postulated that the length of the rope of the velocity meter is constant - which was not always the case during the total duration of the campaign).

Following from the neap-spring variation, the velocities at the beginning and at the end of the measuring campaign should be fairly equal, although the spring tide around August the 12th was larger than around July the 28th. The maximum ebb velocities are more or less equal, but the maximum flood velocities differ 1 m/s.

The depth of the meters is approximately 1.6 m and 1 m, which also indicates that the velocities in August were larger. The tidal range in August is larger than that of July, thus more water has to be moved during ebb or flood within the same timelaps in August. Consequently, the velocity is higher.

Conclusions:

The depth of the velocity meter does not influence the magnitude of the velocity significantly and the discrepancies of the depths are caused by the uplifting of the flow. A restriction to this statement is that the meters are not located near the bottom, where the velocity gradient is usually higher than up in the vertical. Near the bottom, a change in depth will have more effect. The measured velocity can be used as mean velocity, with which the velocity profile is determined (see ***equation (2)*** in ***section 4.2***).

The velocity varies as a result of the neap spring variation, which is shown in ***table 2.8***. A correction for the neap-spring variation is necessary.

Table 2.8

I–A	max. ebb velocity [m/s]	max. flood velocity [m/s]
neap	0.8	1.1
spring	1.6	3.1

§ 2.2.3 Comparison between the flow velocities in the cross sections and in I-A

Comparing ***table 2.3 and table 2.4, appendix 2.2***, the influence of the neap-spring variation can be eliminated from the velocity records of the locations, other than I-A.

The velocity at I-B is slightly higher than at I-A and the velocity at I-C is lower than at I-A. The measurements took place on successive days with increasing maximum velocities in I-A. The velocity at I-C is consequently lower than the velocities at the other locations. At section II, the measurements took place during increasing tidal ranges, which results in increasing velocity maxima. In general, the velocities are lower than in I-A. The velocities in III-A and III-B decrease, following the diminishing tidal range.

Comparing the maximum and minimum velocities, the locations in section I, and II-A are situated in a flood channel, whereas locations II-B, III-B and KP8 display maximum ebb and flood velocities, being more or less equal. Locations III-A, III-C, TRW and II-C are situated in ebb channels. This is confirmed by the results from the float tracks.

§ 2.3 Temperature

The temperature in I-A is approximately 30^{0}C, varying slightly between night and day. The temperature influences the kinematic viscosity and the density of the water. Both values are assumed to be constant in time.

§ 2.4 Sediment concentrations

The sediment concentration in the water is measured at three locations, one location per cross section. The figures, found in ***appendix 2.1***, depict the water levels, the velocity and a graph of the concentration at the bed and at the water surface. The samples were taken in the locations:

I-A (***figure 2.4.1***) at: 27/07/91
II-A (***figure 2.4.2***) at: 07/08/91
III-B (***figure 2.4.3***) at: 01/08/91

The locations I-A and III-B were sampled around the spring tide, but II-A was sampled just after the neap tide. ***Table 2.9*** displays the minimum and maximum concentrations in the locations.

Table 2.9 Minimum and maximum concentrations in mg/l

location	bottom		surface	
	minimum	maximum	minimum	maximum
I-A	450	2800	220	1000
II-A	200	1400	50	1000
III-B	250	2600	60	750

§ 2.4.1 Concentrations in I-A:

The concentrations fluctuate considerably. The samples were taken from the pontoon, under high flow velocity conditions, with a maximum velocity of 2.5 m/s. It was therefore difficult to perform the sampling. The sampling in the other locations took place from a drifting boat, reducing the forces on the Niskin bottle.
The concentration near the bed follows the fluctuation of the velocity, except between 8.00 hrs and 12.00 hrs, during flood, when the highest velocities occur. This is when the concentration near the bed is equal to the surface concentration, which indicates a well mixed concentration vertical. This is probably caused by the turbulent flow coming from deeper parts of the estuary on the sea side of I-A.

The minimum concentration occurs just after slack water, putting aside the concentrations from 8.00 hrs to 12.00 hrs. The surface concentration on the contrary fluctuates between 1000 mg/l and 220 mg/l, with a gust of 1400 mg/l. The minimum concentration occurs before slack water, which is remarkable.

§ 2.4.2 Concentrations in II-A:

The shape of the concentration curve in time is smoother than in I-A. The lowest concentrations occur half an hour after slack water. The concentration decreases gradually at the end of the flood and the concentration increases during ebb, but show a backsliding in concentration between 13.00 hrs and 15.30 hrs similar to that at I-A, though the flood velocity is higher than the ebb velocity. Just as in I-A, the difference between the bottom and the surface concentration is smaller than during flood. In contrast with I-A, this phenomena occurs during ebb, instead of during flood.

§ 2.4.3 Concentrations in III-B:

The form of the curves are gradual, except for the backsliding around 11.30 hrs. The lowest concentrations occur after slack water, whereby the surface concentration is more retarded than the bottom concentration. It is shown that the sand is lifted from the bed and hence carried in upward direction.

The concentrations during slack water after high water are lower than after low water, because the water depth at high water slack is maximal, thus the sediment can sink from the upper layer. At low water slack, the depth is minimal, so the sediment remains better mixed over the vertical.

The concentrations of III-B are used in ***chapter 5*** for calibration of a model, that calculates the concentrations in one position. The data obtained in the other locations were not suitable, because of the fluctuations in the data of I-A and the fact that section II is situated near the bar, which causes a flow field which is not typical of the whole area.

§ 2.4.4 Comparison

The concentration near the bed in II-A is quite low, compared to the concentration at the other locations, as a result of the lower velocity in II-A. The velocity is low because of neap tide and the short interval between the sampling, which only includes the ebb phase of the tide and not the flood, where the velocities run up to 1.5 and 2.0 m/s. The difference between the surface concentration and the concentration near the bed is large in I-A and III-B, in contrast to II-A. This is a result of the smaller depth in II-A (near the bar), where the sediment is better mixed over the vertical.

§ 2.5 Density of the water

The density of the water is determined by application of a density float. The maximum and minimum values are displayed in ***table 2.10***.

Table 2.10 Water density

location	maximum density [kg/m^3]	minimum density [kg/m^3]
I-A	1000	998
II-A	999	997.5
III-B	999.5	998

The densities are all in the same order of magnitude and are lower than the usual 1000 kg/m^3 for fresh water, because of the high temperature. It is assumed that there is only a small amount of salt intrusion in this area, because the density of fresh water of 30^0 C is 995.68 kg/m^3. The densities, corrected for the sediment concentration do not differ much from the density of fresh water of 30^0 C. The densities do not vary much in time or in depth, so it is assumed that the effect of density currents, caused by either differences in the sediment concentration over the vertical or salt intrusion in this area can be neglected.

§ 2.6 Soil samples

In most locations, a soil sample is taken with a van Veen grab. Within the framework of this study, these samples were dry sieved, after being wet sieved to eliminate the fine fractions. The smallest diameter that can be selected by standard sieves is 63 mm. The bed material of the Hooghly is very fine, so is was not easy to determine reliable grain size distribution curves. Parts of the soil samples, that were taken I-B, II-B and III-B, located in the channel axis, were sent to an external geotechnical laboratory to determine the grain size distribution curves.

The grain size distribution curves could not be determined quantitatively, but the different locations per cross section at different days can be compared. The distribution curves that were determined by the geotechnical laboratory are more reliable. ***Figure 2.1 in appendix 2.1*** shows the days of sampling with regard to the neap spring variation.

Comparison of grain sizes within the cross sections

In cross section I, the grain sizes in I-B are smaller than in the other locations, although the samples in I-B and I-C were taken on the same day.

The grain size distribution in cross section II of II-A and II-C vary, the grains in II-C being coarser than in II-A. The orientation of both locations with regard to neap tide is quite the same. According to ***table 2.3, appendix 2.2***, the velocities in II-A are higher than those in II-C. With regard to the diagram of Hjulström [Nortier, 1961], a higher velocity is required in order to entrain bed material of smaller grains in the part of the diagram for grain sizes below 300 μm. Under

lower flow conditions, (relatively) coarse material is not yet eroded. This could be an explanation.

In cross section III, the material in III-B seems to be slightly coarser than in III-A, but the sampling in III-A took place closer to the spring tide (higher velocities) and shorter after the storm on 28/07/91.

Comparison of grain sizes between the cross sections

From the curves, the coarsest material is found in II-B near the bar and the finest material in I-B. The velocities in II-B are relatively low, so the coarse material can not be held in suspension and settles.
The maximum velocities in the locations on the day of the sampling:

I-B:	2.7 m/s
II-B:	1 m/s
III-B:	1.7 m/s

This explains the presence of the finest material in I-B. The samples of I-B and III-B are obtained around spring tide and that of II-B around neap tide, which results in low velocities in II-B.

Table 2.11 displays the characteristic grain diameters.

Table 2.11

Characteristic grain sizes in mu determined by laboratory

Location	D10	D20	D30	D40	D50	D60	D70	D80	D90
I–B		4	10	18	25	33	44	55	89
II–B	79	100	112	122	133	145	150	177	196
III–B	37	55	72	83	95	107	119	132	146

Characteristic grain sizes in mu obtained by sieving in framework of study

Location	D10	D20	D30	D40	D50	D60	D70	D80	D90
I–B									88
II–B	84	104	120	137	153	165	177	190	202
III–B							72	109	142

Chapter 3 Harmonic analysis of tides

Introduction

A computer programme that computes the flow field and the sediment concentration field, needs tidal flow data as a boundary condition for the computation.
During the measuring campaign a large number of water level registrations were obtained, but this cannot be put into the model, when predictions of the measuring range of the tide need to be given as well. Therefore, a function is fitted to this data.

The data was obtained from the following Indian water level registration stations:

Gangra Semaphore
Oil Jetty Station
Balari Semaphore
Diamond Harbour Station

The orientation of the registration stations with regard to the area of interest is shown in ***figure 1.2.3.1.*** All figures in this chapter can be found in ***appendix 3.1*** and all tables are in ***appendix 3.2.*** The stations closest to the area of interest, which is to be schematized in the programme, are the Oil Jetty and Balari Semaphore.

The registrations of the Oil Jetty have been chosen to be examined, because the registrations seemed the most reliable. Moreover, the tide is only influenced by tidal streams in Haldia Channel, in contrast to the Balari Semaphore where the Rangafalla Channel also influences the tidal movement. Nor is it precisely known where the registrations of the Balari Semaphore took place exactly, because the registration drum was connected to a pressure box via a tube on the river bottom, leading approximately a thousand meters up the river.

At the Oil Jetty, the water level is detected by a float in a tube. In the tube, the short waves are subdued, so only the long period waves are registered. A mechanism registers the level on a drum, on which a piece of paper is attached. From this output, the water level is read and registered every half hour by an attendant of the Calcutta Port Trust. The level at high and low water is recorded as well.
The data was checked for typing errors, made during registration. This was done by checking the signal on unusual peaks.

§ 3.1 Theory

There are two methods of examining a tidal movement:

-a: The harmonic analysis:
the amplitude and phase angle of a number of components with known frequencies are computed, using the method of least squares

-b: The spectrum analysis:
the spectrum is divided in small ranges of the same width. In this way, many frequencies are generated. With these frequencies,

Fourier components are developed and the amplitudes and phase angles are computed. The frequencies, plotted against the amplitudes concerned, show an energy distribution of the total tidal signal, that indicates where the significant frequencies are located.

The advantage of the harmonic analysis is that a better insight is gained in the physical mechanism of tidal movement, because the actual harmonic components are used. This method however, does not give any indications of the length of the observation interval and the time step. The spectrum analysis supplies information on the whole frequency interval and provides conditions for the observation interval and time step.

To gain more insight, the harmonic analysis is chosen for application, but to make an estimation of the time interval and time step, the demands of the spectrum analysis are used. The latter analysis is also used to sort out the significant frequencies of the signal.

§ 3.1.1 Origin of tidal movement

The purpose of a harmonic analysis of tides is to obtain a formula which fits the tidal movement data in one location. The moon and the sun are the most important driving forces of the tide on earth. As a result of the centrifugal and attracting forces, a resultant shear force along the surface of the earth occurs [Kalkwijk, 1983]:

$$F_s = [\frac{3Mg}{2K^2}] * \sin(2\theta)$$

g = 9.81 m/s^2
M = mass of the moon / mass of the earth
K = distance earth-moon /radius earth
θ = angle between earth radius of location at the equator and earth radius of the location in which the shear force is determined

This can be written as follows:

A $\cos[(i*\omega_a' + j*\omega_m + k*\omega_z + l*\omega_p + m*\omega_k + n*\omega_l)*t + \Theta]$, whereas $\omega_a' = \omega_a - \omega_m$

All harmonic and shallow water angular frequencies in ***table 3.1*** are calculated from given combinations of i,j,k,l,m,n; ω_a up to ω_l are known values.
These ω's are angular frequencies effected by the following factors: the earth, the moon, the sun, the rotation of the ellipse of the moon, the rotation of the plane of the moon orbit, and the precession of the earth-axis.

§ 3.1.2 Length of the observation interval

In a tidal analysis, different frequencies interfering with each other should be avoided, because only then will it be possible to distract the different components from the tide in a proper way. The criterion of Rayleigh requires that the relative change in phase between two harmonic waves is at least 2 π rad.

$$| \sigma_{j+1} - \sigma_j | = 1/[(2N + 1)*\Delta t] \approx 1/(T)$$

T	=	observation interval
Δt	=	time step
σ_j	=	frequency at time is j*Δt
2N+1	=	total number of time steps, N in positive direction, N along the negative direction of the time axis and zero makes 2N+1

From the list of harmonic components, a number of important frequencies were chosen to determine the length of the observation interval. ***Table 3.2*** displays the angular frequency and the frequency of the components; ***table 3.3*** shows the minimum observation time needed to divide the combinations of frequencies. The frequency can be calculated from the angular frequency via:

$$\omega = 2\pi/T \text{ and } \sigma = 1/T$$

wherein	ω	= the angular frequency,
	σ	= the frequency and
	T	= the wave period.

The observation interval required to separate the K_1-component from the P_1-component is too long (almost a year), so only one of these components, K_1, will be used in the analysis. K_1 is preferred over P_1, because the amplitude on deep water of K_1 is larger than the amplitude of P_1. (Amplitude of K_1 = 0.53 m, P_1 = 0.18 m, [Kalkwijk, 1983])

According to ***table 3.3***, it can be concluded that the longest requested observation interval has to be more than 31.81 days; an observation time T of 53 days was therefore chosen. It is better to chose a long observation interval, because the disturbing effect of incidental storms on the determination of the tidal components will be less.

$$\Delta\sigma = 1/T$$

$$\Delta\omega = \Delta\sigma*360°$$

According to the above mentioned formulae (after substituting T) the difference between frequencies that can be separated must be bigger than 0.0008 hrs^{-1}. Therefore, following from the second formulae, the $\Delta\omega \geq$ 0.2830 dgr/hr.

§ 3.1.3 Determination of the time step

To avoid aliasing, the time interval is restricted to a certain maximum. When aliasing occurs, one certain frequency is recognized as a lower frequency. This certain frequency is mirrored over a fault frequency. Aliasing will not occur if the fault frequency is the highest frequency that occurs in the spectrum.

$\sigma_{2(MS)8} = 0.3277$ hrs^{-1} is chosen as a maximum frequency, because $2(MS)_8$ is the highest angular frequency of ***table 3.1***. The sample interval is determined according to:

$$\sigma_f = 1/(2\Delta t) \qquad \sigma_f = \text{fault frequency}$$

This provides a sample interval of $\Delta t = 1.5$ hrs. The applied sample interval is $\Delta t = 0.5$ hr.

The data is fitted with a Fourier series of the following form:

$$h(t) = h_0 + \sum A_n * \cos(\omega_n * t) + \sum B_n * \sin(\omega_n * t)$$

with: $A_n = h_n * \cos \alpha_n \quad n = 1,2,3,\ldots$
$B_n = h_n * \sin \alpha_n \quad n = 1,2,3,\ldots$
$h_0 =$ mean water level

§ 3.2 Working method

There are many harmonic and shallow water angular frequencies that can be introduced in a Fourier series (see ***table 3.1***), but they are not all equally important. With the aid of spectrum analysis therefore, the significant angular frequencies are sorted out.

For the calculation of the harmonic components and for the spectrum analysis a statistical calculation programme (SPSS) is used. This programme requires an input file of time and matching water levels.

A chosen angular frequency set is inserted and the programme calculates the variables, according to the Fourier series, with the aid of the method of least squares. Much statistical output can be obtained optionally, helping to sort out the best fit from several angular frequency combinations and detecting dependencies between the angular frequencies. Dependency must be prevented, because it gives inaccurate results.

The question arose, if the tidal amplitudes and the mean water level change during different times of the year, for example during the monsoon and the dry season. To answer this question, two sets of data were fitted, one set of data during the monsoon and one during the first measuring campaign (March/April).

§ 3.3 Spectrum analysis

§ 3.3.1 Angular frequency ranges

Table 3.1 shows a variety of components that occur frequently. The components are divided in harmonic components that are a result of interacting forces of astronomical origin, and shallow water components resulting from non-linear phenomena such as bottom shear stress and variable propagation velocity, which is depth-dependent. The bathymetry of the area also influences the shape of the tidal wave, but this can not be reflected by angular frequencies.

Looking at ***table 3.1***, some angular frequency ranges can be distinguished, in which many angular frequencies were found, named respectively the first range, the second range and so forth. The angular frequency range before 12.85 is also investigated, as the MS_f and other long period waves are found there.
For spectrum analysis, the angular frequency ranges are divided in n steps of $\Delta\omega$. $\Delta\omega$ must be at least 0.2830 (***section 3.1.2***) to avoid dependencies between angular frequencies. By taking steps of $\Delta\omega = 0.3$, $n+1$ angular frequencies are created, that are put in the calculation programme. The matching amplitudes can be derived from the output of the programme.

Because these angular frequencies are not exactly the angular frequencies of the harmonic and shallow water components, the amplitudes give an estimation of the real amplitudes only. Yet, if the amplitudes and angular frequencies are plotted against each other, this gives an indication of where the significant angular frequencies are situated in the angular frequency range.

This was done for all the angular frequency ranges for the monsoon period and the period in March/April, in order to check if there is a change in important angular frequencies during the year.

Figures 3.3.2.1 up to 3.3.2.12 show the amplitudes plotted against the angular frequencies for the March/April period and the Monsoon period. The spectrum in between the angular frequency ranges are also investigated on important angular frequencies, but none were found.

§ 3.3.2 Processing of the output of the spectrum analysis

From the plots of the angular frequencies against amplitudes, the angular frequencies with an amplitude bigger than 0.05 m were selected to be put in the harmonic analysis. The value 0.05 m was chosen because an amplitude of less than 0.05 m does not have much influence on the signal with an average tidal range of about 4 m (1.25 %). This criterion, however, can be changed if it does not suffice.

Two particular situations can occur:

-1 If two adjacent angular frequencies come close to the amplitude of 0.05 m, this small range is also investigated, because a harmonic angular frequency can occur in between both angular frequencies, resulting in an amplitude of more than 0.05 m.

-2 If two harmonic angular frequencies near a frequency with an amplitude more than 0.05 m differ less than 0.3, only one of them can be implemented in the calculation. By looking at the amplitudes on deep water of the harmonic angular frequencies [Kalkwijk, 1983], the angular frequency with the largest amplitude is chosen.
Since only the amplitudes on deep water of the harmonic components are known, the choice between shallow water angular frequencies is made by putting the two angular frequencies in a (separate) calculation and selecting the one with the highest amplitude.

Table 3.5 shows the frequencies, following from the spectrum analysis, that caused an amplitude of more than 0.05 m, during both observation periods. The fourth column presents the harmonic or shallow water components that are assumed to be the cause of the increased amplitudes. These components are preferred over the components of the fifth column, because of the reasons mentioned at point 2.

In order to gain a better insight in the impact of a certain angular frequency range on the tide, the residue of the signal after subtracting the signal of the separate angular frequency ranges is shown. The ***figures 3.3.2.13 up to 3.3.2.16*** display the residue of the total time period and the residue of three days of the time period for the first four angular frequency ranges. The rest of the ranges did not alter the signal much, so the residue is not shown.

§ 3.3.2.1 First range

The K_1-component is preferred over the other harmonic components of the range 14.8-15.1, because the highest amplitude of 15.1 indicates that the angular frequency must be near 15.1 and the K_1-component has got the largest amplitude on deep water [Kalkwijk, 1983]. These components were entered into the programme and were checked to see if their amplitudes were still above the 0.05 m criterion.

The first angular frequency range levels out the daily inequalities of the tide, so the outer line along the tidal signal becomes smoother. See ***figure 3.3.2.13***.

§ 3.3.2.2 Second range

The second angular frequency range (***figures 3.3.2.3 and 3.3.2.4***) appears to be very important when simulating the tidal signal, because the contribution of this range to the total tidal amplitude is considerable.

The large influence of the second angular frequency range is seen in ***figure 3.3.2.14***: the amplitude has decreased a lot. The residue is quite irregular.
The computer programme only seems to eliminate the second angular frequency range over complete periods of about fourteen days and leaves out the time intervals at the beginning and at the end of the signal.
This is a boundary effect of the calculation by the computer model, which is tried to be eliminated by equalizing the signal at the beginning and the end of the observation period (see ***section 3.6***).

§ 3.3.2.3 Third range

The amplitudes of the angular frequencies in this range do not pass the 0.05 m criterion (see ***figures 3.3.2.5 and 3.3.2.6***), thus this range is not taken into account in the harmonic analysis.

The impact of the third angular frequency range on the simulation of the tidal signal is not significant (see ***figure 3.3.2.15***).

§ 3.3.2.4 Fourth range

This range contains a lot of significant frequencies that are displayed in ***table 3.4.*** Looking at ***figure 3.3.2.16*** it shows that the fourth angular frequency range are shallow water components, which is shown at the lower edge of the residue: the difference between neap tide and spring tide is smaller than in the residues of the other angular frequency ranges. The residue at low water is flattened in the second picture.

§ 3.3.2.5 Fifth and sixth range

In these higher angular frequency ranges, only the angular frequency 87.9 in the fifth range during March/April can be appointed as a significant frequency (see ***figures 3.3.2.9 up to 3.3.2.12***).

Runs with the calculation programme showed that the 2 MS_6 is responsible for the amplitude.

§ 3.3.2.6 The range below 12.7 dgr/hr

In this range, just a few harmonic components exist, but it is also verified on significant frequencies. ***Figures 3.3.2.17 up to 3.3.2.19*** show the amplitudes plotted against the angular frequencies of the Monsoon period.
The amplitude of 0.3 dgr/hr is not reliable, because its value is too close to zero. (The value of $\Delta\omega = 0.2830$ is also the lowest acceptable angular frequency that can be introduced in a Fourier series). The same analysis during March/April results in a high amplitude adjacent to 0.5 degr/hr.

The values 1.5 and 2.7 degr/hr only gave amplitudes just above 0.05 m during the Monsoon and not in the March/April period. Later on, the same angular frequency set was selected for both periods, because the spectrum analysis resulted in the same harmonic and shallow water components for both periods. Both of the above mentioned values were therefore excluded from the harmonic analysis. Moreover, no harmonic components exist that have values that come close to these frequencies.

§ 3.4 Harmonic analysis

Introduction

The results from the spectrum analysis, combined with ***table 3.1***, gave indications of the significant angular frequencies. These angular frequencies were implemented in a harmonic analysis. Some extra components were added to the selected components. These extra components were chosen nearby angular frequencies with an amplitude of about 0.05 m.

§ 3.4.1 Selection of a suitable angular frequency set

The amplitudes and phase angle of an angular frequency set of 22 harmonic and shallow water components were determined by using the calculation programme. The results are shown in ***table 3.6***. Applying the criterion of the minimum amplitude, several components need to be left out of the set (compare ***table 3.5*** to ***table 3.6***).
The elimination of the MN_4 and S_4 components happens by virtue of the fact that the amplitude in one period does not satisfy the criterion. Now, still 12 components remain.

These 12 components are again put in the calculation programme for both periods, which results in amplitudes that meet the needs of the criterion. The outcome of this calculation is discussed in the following paragraph.
Comparing ***figures 3.4.3.13 up to 3.4.3.15*** with ***figures 3.4.1.17 up to 3.4.1.19***, the latter figures being the result of the calculation with 22 components, it can be said that the latter calculation fits better at low water than the calculation with 12 components.

§ 3.4.2 Discussion of the results of the harmonic analysis

As shown in ***table 3.6***, several striking differences between the two periods are to be noticed:

-1 The mean level in the monsoon period is about 3.50 m, whereas the mean level during March/April is about 3.00 m; a difference of 0.5 m;

-2 Amplitudes of the harmonic components, having undergone a significant change, are:

- M_m: in March/April significantly larger than during the monsoon
- N_2 and L_2: during the monsoon significantly larger in March/April
- S_2: During the monsoon 0.68 m and in March/April 0.87 m

-3 The difference between successive high water periods during the monsoon is bigger than during March/April. This can be explained by the magnitude of the O_1 and K_1 components of both periods.

The rise of the mean level during the monsoon can be explained by the increase of the discharge of the river, caused by the heavy rainfall during the monsoon. Moreover, the prevailing south western winds may drive up the water level. During March/April, the wind blows in the opposite direction and is weaker.

Data of the seasonal changes in mean water level [ATT, vol.2, 1991] shows that this change can be seen as a periodical phenomenon with a period of one year. The amplitude of that signal is about 0.3 m in the area of Diamond Harbour and 0.6 m near Calcutta. In March/ April the wind direction changes from north east to south west. The change in the opposite direction occurs in November. If the mean level on the river is merely influenced by the rising of the sea (caused by sett-up), the effect of the rise will be noticeable only for some period of the year in Calcutta. The discharge of the Hooghly is a result of the monsoon rains, which are caused by south eastern winds that make clouds rise against the Himalayas. Therefore, the significant discharge occurs at the same time (may be a month retardation time) as the south eastern winds that set up the sea level.
The amplitude of the seasonal mean level rise is bigger in Calcutta than in the mouth of the estuary. This means that the river is also an originator of the mean level rise.

According to the statistical output, the differences in amplitude of several angular frequencies are a result of the increased dependency of the components. If one adds the amplitudes of the N_2, L_2, and S_2 for both periods, resulting amplitudes of 1.12 m and 1.11 m are obtained. This means that the total impact of the second angular frequency range is constant and therefore, it is not likely that the differences in amplitude between the two periods are a result of a change in significant angular frequencies in time. This problem will be reviewed in ***section 3.5***.

§ 3.4.3 Explanation of the figures

The measured signal

In ***figure 3.4.3.1***, the tidal signal in March/April is shown. The signal is very regular in comparison to the tidal signal in ***figure 3.4.3.4*** of the monsoon period. This signal shows irregularities, such as elevation of the mean level, which is caused by storms (checked in the journal of the measuring campaign). At the top of the signal, the daily differences are bigger, which explains the larger amplitudes of the O_1 and the K_1 components in the monsoon calculation.

The predicted tidal movement

Figures 3.4.3.2 and 3.4.3.5 show the simulation of the tidal signal by the selected harmonic components. Because of the regular form of the March/April period, the estimated signal looks rather the same. In the monsoon signal however, the irregularities are levelled out; the form has changed slightly, especially at low waters of the signal during a few days of storm.

Figures 3.4.3.3 and 3.4.3.6 give an impression of the overlap of the fit; they show the tidal signal, the predicted signal, and the residue during three days of the respective observation intervals.

The residue

Figures 3.4.3.7 and 3.4.3.10 show the residues of the total observation intervals. The residue still seems to exist of harmonic components, but it was impossible to distract other significant angular frequencies to make the periodical part of the residue disappear. This can be a result of the overestimation of the amplitudes of the components, which is reflected in the residue.

It can be judged from ***figure 3.4.3.7*** that the peaks are higher during spring tide, when the amplitudes amplify each other; ***figure 3.4.3.10*** displays a more irregular residue, with evident elevation of the waterlevel in two cases, at about $t = 600$ hrs and $t = 900$ hrs, due to storms.

The monsoon period is better schematized by the angular frequencies, but because of the storms the signal is more disturbed. According to the statistical output of the calculation programme, the standard deviation is therefore slightly bigger. ***Pictures 3.4.3.8 and 3.4.3.11*** show the residues of the signal during three days. In ***picture 3.4.3.9 and 3.4.3.12***, the computed fit can be seen in this period.

The influence of the neap and spring tide variation

In order to compare the quality of the fit during different periods of the fortnightly tidal movement, ***picture 3.4.3.13 up to 3.4.3.18*** show the measured and predicted signal and the residue of spring tide, neap tide and the period in between of

respectively the March/April period and the monsoon period. The spring tides and mean tides are easier to predict than neap tides. The ebb and flood time intervals are well matched, but during high water and especially during low water, both lines do not coincide. During low water, the water retreats because of shallow water effects.

The shallow water effects

There are two effects caused by the shallow water effect. Because of the lower mean level, the propagation velocity reduction is stronger during March/April than during the Monsoon. This can be judged from the residues of ***pictures 3.4.3.13, 14 and 15***, when compared to that of ***pictures 3.4.3.16, 17 and 18***, which show smoother residues. The second effect is that during the spring tide at low water, the lowest propagation velocity occurs. During ebb, flood and high water, the propagation velocity is higher, so shallow water effects are smaller. ***Figures 3.4.3.13 and 3.4.3.16*** show a peak in the residue just before low water, and a dip just after low water. The residues at neap and mean tide are smoother as a result of a smaller tidal range, and consequently, a smaller change in propagation velocity.

§ 3.4.4 Impact of the components on a single tidal cycle

In order to gain insight in the effect of several components of a single tidal cycle, one or more components are subtracted from this signal.
In ***picture 3.4.4.1***, only the M_2 component is subtracted; the graph shows the measured and the predicted signal and the residue. The retardation during low water is significant and the residue shows a distorted harmonic signal.
Picture 3.4.4.2 displays the measured signal as well as a signal predicted by the M_2 and K_1 component. Due to the small data range considered (about 12 hours), the M_2 component influences the S_2 component. For this reason, the S_2 component is not included in the calculation. The amplitude of the residue has become smaller, but the residue looks still like the residue of the first picture.
Picture 3.4.4.3 demonstrates the impact of the M_2, K_1, and the MS_4 components. The amplitude of the residue has decreased considerably and its so-called 'period' has become smaller.
Pictures 3.4.4.4 and 3.4.4.5 show the effect of two added components, M_4 and MN_4 respectively. The amplitude of the residue gets smaller still, but its shape remains unaltered. The predicted cycle fits increasingly better, especially at high water, ebb and flood. There is still a lag in the tide at low water.

Conclusion

The programme is able to make a good fit of one tidal cycle with the harmonic components mentioned above; therefore, it must also be able to fit a longer time period with the same components. The shallow water effect is still present after subtracting three shallow water components; causing the low water part of the cycle to be the most difficult part to fit.

§ 3.5 Short study of dependency of the components

In order to explain the occurring differences between the amplitudes of the components of the second angular frequency range mentioned in ***section 3.3.2.2***, the angular frequencies are divided into two groups, in which the angular frequencies of the same range do not particularly influence each other (see ***table 3.7***).
According to the statistical output of the programme, the marked components are those components that are slightly inaccurate in the calculation. This can cause a considerable variation in the amplitude of the harmonic component. The fourth column shows the amplitudes from the run with all the angular frequencies put together; the sixth column displays the amplitudes of the components after the separated runs.

The separated runs exist of:

first run	second run
MS_f	M_m
O_1	K_1
$2MS_2$	N_2
M_2	L_2
S_2	
M_4	MS_4
$2MS_6$	

The components that gave inaccurate results in the total run, remained inaccurate in the separate runs. The division of the components did not solve the problem of the dependencies. The dependent components are connected as follows:

$MS_f \approx 2 * M_m$
$2MS_2 \approx 2 * O_1$
$S_2 \approx 2 * K_1$
$2MS_6 \approx 3 * L_2$

Most of these combinations in the separated runs are segregated, except for O_1 and 2 MS_2. The inaccuracy is amplified in the separate runs, which can be concluded from the fact that the amplitudes of MS_f in March/April and $2MS_2$ during the Monsoon have become inaccurate in the separate runs.

The changes in magnitude of the other amplitudes are caused by separation of the components. The angular frequencies are computed one by one in the programme. When an amplitude of a new angular frequency is computed, the remainder of the amplitudes are corrected to create a better fit. If the angular frequencies are divided into two groups, the amplitudes are only corrected for half of the angular frequencies, thus these different methods will not lead to exactly the same solution.

The amplitude change of S_2 during the monsoon output is bigger than the amplitude change of the other components, probably because this component has a relatively large amplitude. Therefore, it is more sensitive to corrections. A plausible explanation for the fact that the S_2 component only changes in the monsoon period could be that the whole period of March/April is more accurate during the Monsoon, because of worse weather conditions; also the amplitudes of $2MS_2$ and L_2 have changed.

§ 3.6 Boundary problems

In order to gain more insight into the phenomenon, mentioned in ***section 3.3.2.2***, the following solution to reduce this effect is investigated: two components, simulating the M_2 and the S_2 components, are added (Amplitudes: M_2 = 1.644 m and S_2= 0.678 m, according to the monsoon output of the analysis). Then the components are separated by the programme. The residue showed an almost non-reduced signal at the beginning and the end of the time interval, due to a degree of freedom of the analytical solution.

Next the signal was equalized before entering it into the computer programme. This was done by multiplying the signal by a function, the data window. This data window is built up as follows: the function is applied over the total observation time T, which is divided in three parts. The first part has a length of T_d = 0.2 T, the last part idem and the rest of the period is situated in between. The first part of the tidal window is represented by the function $0.25(1-\cos(\pi*t/T_d))^2$; the last part of the tidal window is found using $0.25(1-\cos(\pi(T-t)/T_d))^2$. The rest of the function exists of a constant function f(t) = 1. This tidal window reduces the amplitudes of the beginning and the end of the tidal signal gradually to zero.

The adjusted signal was entered into the programme; now the boundary problems had disappeared, but the total residue had grown, resulting in a more inaccurate calculation. According to the demand of ***section 3.1.2***, the undisturbed interval was of a sufficient length. Perhaps, another data window will lead to better results. This problem was not further investigated.

§ 3.7 Admiralty Tide Tables

The Admiralty Tide Tables give angular frequencies of the area that are quite equal to the acquired angular frequencies. See ***table 3.8***.
The stations Saugor, Diamond Harbour and Calcutta Kidderpore lie in this order of position upstream the river. The location of the Oil Jetty is situated in between Saugor and Diamond Harbour, it may therefore be expected that the magnitudes of the determined angular frequencies lie in between both stations.

The MS_f component increases fast upstream as does the M_m component. The daily components O_1 and K_1 first increase, but upstream Diamond Harbour, the amplitudes decrease. The diurnal components present the same feature. The maximum amplitude is assumed to be nearer to Diamond Harbour than to Calcutta Kidderpore.

Most of the acquired angular frequencies lie in between Saugor and Diamond Harbour, except for the M_m, the K_1, the N_2, the M_2 and the L_2 components. The cause of the higher amplitudes of the diurnal components is that the amplitudes are overestimated by the calculation programme and the errors in the amplitudes neutralize each other. The overestimation of the amplitude of the Mm is similarly due to a presumed underestimation of the MSf component.

§ 3.8 Conclusions

The tidal signal of the two periods can be simulated by the same set of harmonic and shallow water components, although the amplitudes of the two periods are not the same. Further on, the mean water level of both periods differ 0.5 m.

Therefore, a whole year can not be represented by one single function consisting of the same harmonic components.

It is difficult to fit the signal at low water, because of the shallow water effects, some of which cannot be represented by harmonic components. The geometry has its influence and so does the Rangafalla channel, which is predominantly an ebb channel.

Following from the discrepancy of the observed and fitted tidal signal, the measured flow can not be connected to the fitted signal in order to calculate the sediment transport. Data sets of observed water levels are given as input for the programme.

Chapter 4 Theory of the sediment distribution over the vertical

§ 4.1 Introduction

For the area between Haldia Dock and Kulpi Roads on the Hooghly River, a one dimensional flow model was available and is used by predecessors to reproduce and predict the hydraulic flow conditions in this area. This model is going to be extended by a sediment transport model to predict the sedimentation and erosion.

Sediment transport can be distinguished into bed load transport and suspended sediment transport. Although both transport types take place according to different mechanisms, they can not be strictly separated.
The sediment in the Hooghly river is very fine; therefore, the amount of bed load transport is considered small compared to the suspended sediment transport. Consequently, the bed load transport is neglected and only the suspended sediment transport is taken into account.

A sediment transport model usually exists of a mass balance equation in horizontal direction. The instantaneous velocity and sediment concentration are part of this mass balance equation. The velocity and sediment concentration are depth-averaged quantities.
The sediment concentration can be determined by a model of vertical concentration distribution of suspended sediment for non-permanent flow [de Reus, 1979]. From the output of this programme, the depth-averaged concentration is derived. This is applied together with the velocity to determine the horizontal sediment transport.

In this report, only the model of vertical concentration distribution is applied for the data of the Hooghly River. This model is modified on certain issues. The implementation of these results into the overall hydraulic model is not dealt with.

Assumptions within the model

-1 A depth-averaged diffusion coefficient is used, except for the layer near the bed. This schematization matches the observations of Coleman on data of several rivers.
-2 The bed load transport is neglected compared to the suspended sediment transport, because of the combination of fine material and high flow velocities.
-3 The influence of short period waves is neglected for reasons mentioned on ***page 5*** and because of the reduction influence of mud on the entrainment of sediment by waves mentioned in van Rijn [1990].
-4 Density currents are assumed not to occur in this area as is explained in ***section 2.5***. Consequently, density currents are not taken into account.
-5 In the original programme, the water depth was held constant. This was altered in the course of time.

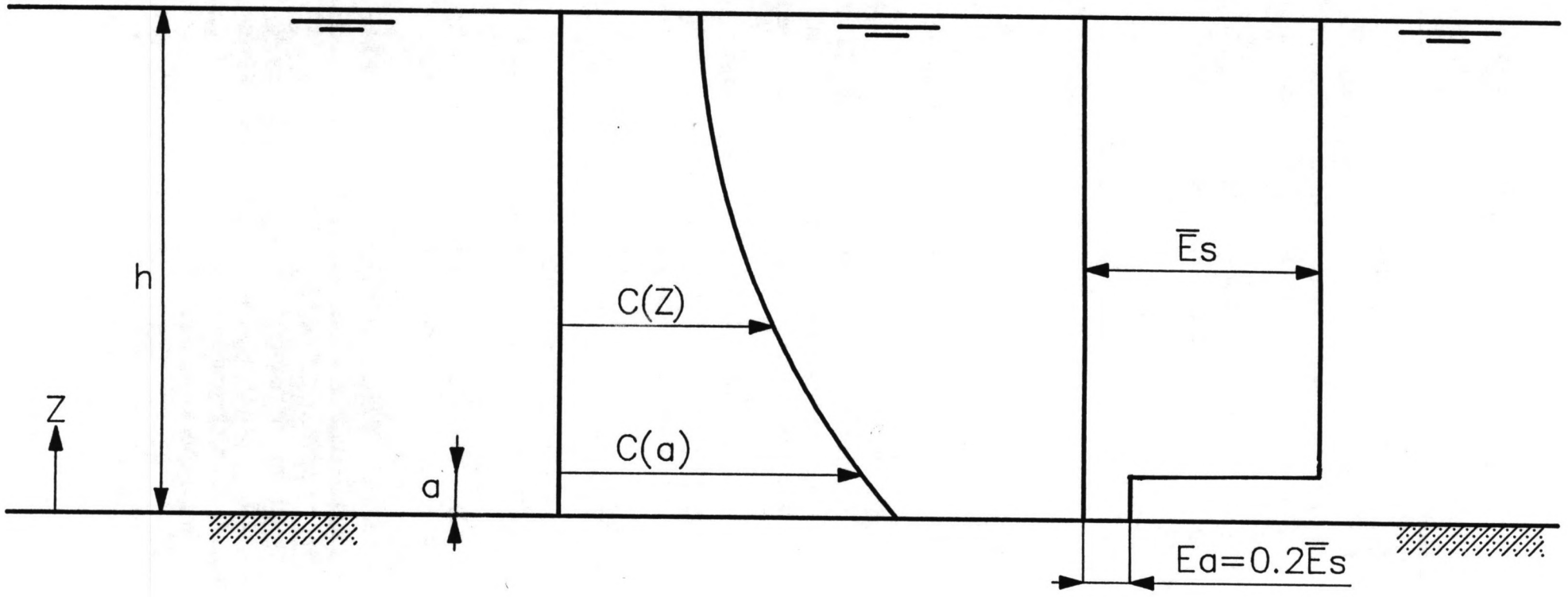

Figure 4.2.1

§ 4.2 Theory

A short description of the theory, on which the programme is based, is written below. More detailed information is found in van Kooten [1974], Prins [1977] and de Reus [1979].

Concentration profile

At the start of the calculation, a concentration distribution under permanent flow conditions is assumed, according to the following formula:

$$c(z) = c_a \cdot e^{-\frac{w}{\varepsilon_s}(z-a)} \qquad (1)$$

wherein:

c(z) = sediment concentration on height z above bed level
c_a = concentration on height a above bed level
w = fall velocity of the sediment
z = height above the bottom (vertically)
a = height above the bottom (small)
ε_s = (depth-averaged) diffusion coefficient

The shape of the concentration distribution over the vertical and the schematization of the diffusion coefficient used within the programme are shown in figure 4.2.1. For the time being, the formulae will be derived for any diffusion coefficient.

Velocity profile

The vertical velocity distribution is represented by the following logarithmic equation, formulated by Keulegan [Graf, 1971]:

$$v(z,t) = [1 + (\frac{v_*}{\kappa \cdot \bar{v}(t)}) \cdot (\ln(\frac{z}{h}) + 1)] \cdot \bar{v}(t) \qquad (2)$$

wherein:

v_* = $v_*(t)$ = shear stress velocity
v(t) = depth-averaged velocity

Diffusion equation

The diffusion equation is applied for the total depth. Boundary conditions are defined for the layer at the water surface and the layer near the bed. They are mentioned below. The diffusion equation:

$$T_v = -w.c - \varepsilon_s . \frac{\partial c}{\partial z} \qquad (3)$$

in which:

T_v = vertical sediment transport
E = entrainment factor, which represents the amount of exchange of sediment between the bed and the water above the bed
dc/dz = concentration gradient.

Continuity equation

The change in concentration in time follows from the change in vertical sediment transport over the height:

$$\frac{\partial T_v}{\partial z} + \frac{\partial c}{\partial t} = 0 \qquad (4)$$

Boundary conditions

The boundaries are located at the water surface and at the bed. No vertical sediment transport occurs at the water surface, resulting in $T_v=0$ at the surface.

The diffusion equation in the vertical direction serves as boundary condition near the bed in the following form:

$$T_v = E - w.c - \varepsilon_a . \frac{\partial c}{\partial z} \qquad (5)$$

with:
ε_a = diffusion coefficient in the lower part of the vertical ($z < a$)

The entrainment factor E is added to the diffusion equation concerning the layer near the bed. This layer should be of limited height, that is not larger than h/20, for which a reduced diffusion coefficient is valid. The entrainment factor can be seen as a kind of production term at the boundary: the amount of sediment being in suspension increases and decreases according to the entrainment factor.

Entrainment factor

Equation (5) contains an extra term compared to equation (3), the entrainment factor. As described below, a formula for the entrainment factor, independent of the concentration is derived:

$$E = e^{[1.99\ln((\frac{v_*}{v_{*cr}})^2 - 1) - 3.97]} \quad (6)$$

According to the theory, the entrainment factor can be written as:

$$E = 0.8\ c_a . w \quad (7)$$

The diffusion equations are made continuous at height z=a above the bed by putting:

$$(\frac{\partial c}{\partial z})_{equation(3)} = (\frac{\partial c}{\partial z})_{equation(5)} \quad (8)$$

Assuming permanent flow conditions during the first time step, no vertical transport occurs at t=0 (T_v=0).

Elimination of $(dc/dz)_{z=a}$ by combining equation (3) and (5), making the diffusion equations continuous, and assuming permanent flow conditions, results in a formulation of the entrainment factor:

$$E = c_a . w . (1 - \frac{\varepsilon_a}{\varepsilon_s}) \quad (9)$$

In the framework of this study, the diffusion coefficient at height z=a is defined as $\varepsilon_a = 0.2\ \varepsilon_s$, ε_s being an average diffusion coefficient over the depth. Therefore, the entrainment factor equals:

$$E = 0.8\ c_a . w \quad (10)$$

The concentration near the bed is calculated in van Kooten [1974], Prins [1977] and de Reus [1979] deriving the total sediment transport S_t from the curves of Coleman. S_t is assumed equal to the suspended sediment transport according to the formula of Lane and Kalinske:

$$S_t = S_1 = \int_0^h v(z).c(z)\,dz = P.q.c_a \quad (11)$$

in which:

S_1 = suspended sediment transport according to Lane and Kalinske
P = f(w/v*,c) = an integral
q = v.h = discharge per m¹

By combining equation (10) and (11), eliminating the concentration c_a, the result is:

$$S_t = P.q.\frac{E}{w.(1-\frac{\varepsilon_a}{\varepsilon_s})} \qquad (12)$$

For every value of S_t, the entrainment factor can be calculated via (12). In this way, the entrainment factor is a function of h, v and D, representing respectively the depth, the velocity and the grain diameter. The integral P of Lane and Kalinske is corrected, because the diffusion coefficient, which was used to appoint integral P, does not agree with observations. The entrainment factor E is plotted against the term:

$$[(\frac{v_*}{v_{*cr}})^2 - 1] \qquad (13)$$

wherein:
v_* = the shear stress velocity
v_{*cr} = the critical shear stress velocity, which is a function of the grain characteristics

From several researches, described in Dyer [1986], a dependency is assumed between the entrainment factor and the term (13).
On double logarithmic scale, the curve exists of an almost vertical line, passing into a horizontal line. The first part of the curve is put in the following expression, which is used in the programme:

$$E = e^{[1.99\ln((\frac{v_*}{v_{*cr}})^2 - 1) - 3.97]} \qquad (14)$$

§ 4.3 Numerical approximation of the continuity equation

In order to discretize the continuity equation, the vertical sediment equations must be discretized as well.

The water depth is divided into m layers (= Δh) of the same thickness. The concentration in such a layer is defined in the middle of that layer and the vertical transport over the boundaries of the layers are defined at the boundary (as seen in ***figure 4.3.1***), thus the concentrations and vertical transports are not defined in the same grid point (staggered grid). The staggered grid was used in order to schematize the sediment transport model similar to the flow model.

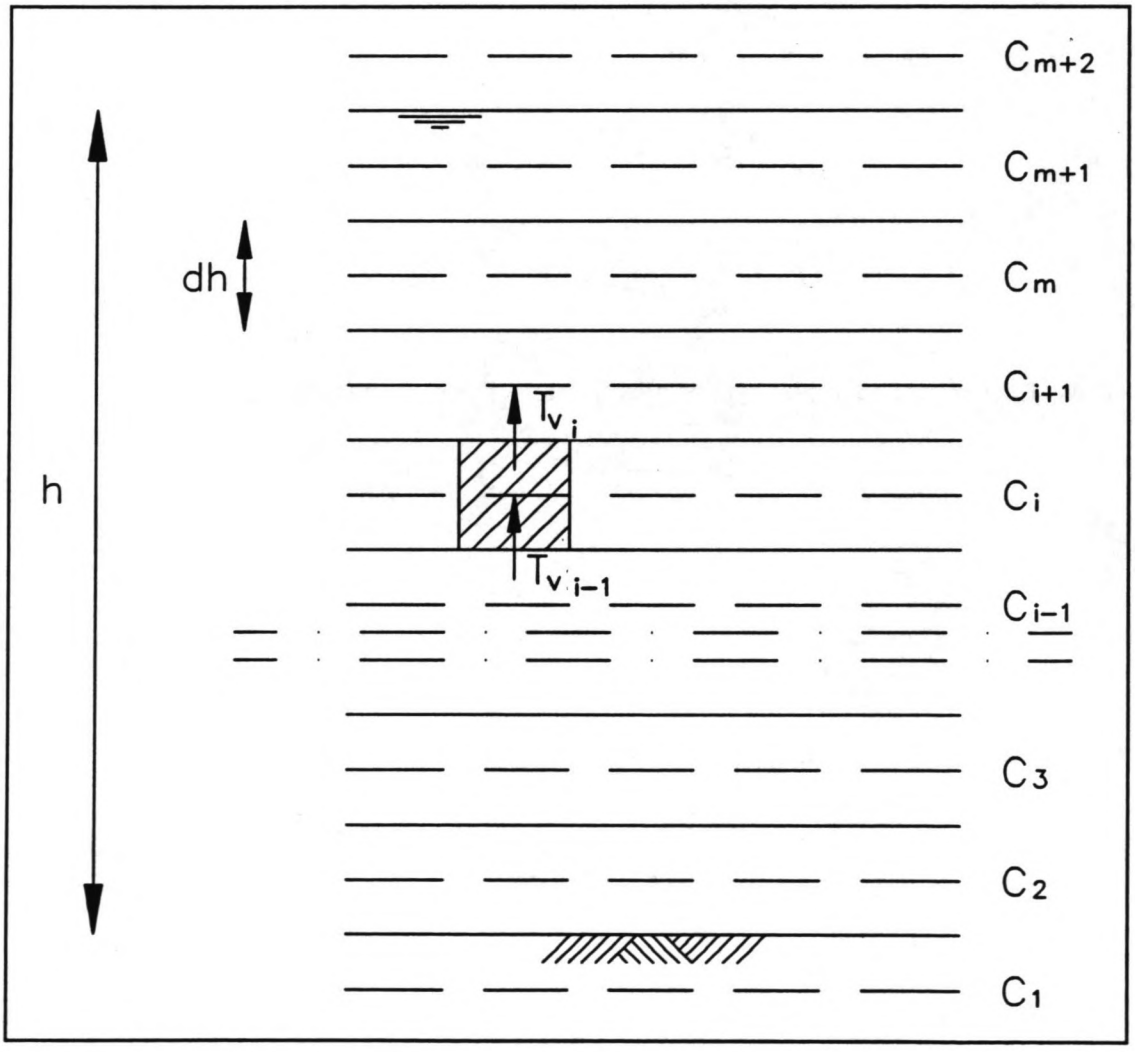

Figure 4.3.1

Assuming permanent flow conditions at t=0, ***formula (1)*** for the initial value of the concentration is discretized as:

$$c(i) = c(2).e^{\frac{-w.\Delta h.(i-1.5)}{\bar{\varepsilon}_s}} \qquad (15)$$

whereas:

i = rank of layer, corresponding with ***figure 4.3.1***
Δh = thickness of the layer
c(2) = c_a = concentration on a height of 0.5 Δh above the bed

The diffusion equations of the hatched block in ***figure 4.3.1*** are discretized as explained below:

For the concentration gradients apply:

$$(\frac{\partial c}{\partial z})_{layer\ i-1} = -\frac{c(i-1)-c(i)}{\Delta h} \qquad (16)$$

$$(\frac{\partial c}{\partial z})_{layer\ i} = -\frac{c(i)-c(i+1)}{\Delta h} \qquad (17)$$

The vertical sediment transport in layer i-1 and i can be written as

$$T_{v\,i-1} = -w[\frac{c(i-1)+c(i)}{2}] - \bar{\varepsilon}_s[-\frac{c(i-1)-c(i)}{\Delta h}] \qquad (18)$$

and:

$$T_{v\,i} = -w[\frac{c(i)+c(i+1)}{2}] - \bar{\varepsilon}_s[-\frac{c(i)-c(i+1)}{\Delta h}] \qquad (19)$$

The discretized continuity equation reads:

$$\frac{\Delta c(i)}{\Delta t} = \frac{T_{v\,i-1} - T_{v\,i}}{\Delta h} \qquad (20)$$

Alternatively written:

$$\Delta\ c(i) = \frac{\Delta t}{\Delta h}(T_{v\,i-1} - T_{v\,i}) \qquad (21)$$

The ***equations (18) and (19)*** substituted in ***equation (21)***, results in:

$$c(i)_{t=t+\Delta t} = c(i)_{t=t} + \frac{\Delta t}{\Delta h}[\bar{\varepsilon}_s(\frac{c(i-1) - 2c(i) + c(i+1)}{\Delta h}) + w(\frac{c(i+1) - c(i-1)}{2})] \quad (22)$$

A different approach is followed at the bottom (i=2). For i = 1, a fictitious concentration is calculated, c(1), and the used concentration gradients are:

$$(\frac{\partial c}{\partial z})_{z=\Delta h} = -\frac{c(2)-c(3)}{\Delta h} \quad (23)$$

$$(\frac{\partial c}{\partial z})_{z=\Delta h} = -\frac{c(1)-c(2)}{\Delta h} \quad (24)$$

The vertical sediment transports are:

$$T_{v2} = -w[\frac{c(2)+c(3)}{2}] - \bar{\varepsilon}_s[-\frac{c(2)-c(3)}{\Delta h}] \quad (25)$$

and, following from the boundary condition:

$$T_{v1} = -w[\frac{c(1)+c(2)}{2}] - \bar{\varepsilon}_a[-\frac{c(1)-c(2)}{\Delta h}] + E \quad (26)$$

The latter formulae, substituted in the continuity equation, together with $\varepsilon_a = 0.2\ \varepsilon_s$, give a formula for $c(2)_{t+\Delta t}$:

$$c(2)_{t=t+\Delta t} = c(2)_{t=t} + \frac{\Delta t}{\Delta h}[(\bar{\varepsilon}_s \frac{0.2c(1) - 1.2c(2) + c(3)}{\Delta h}) + w(\frac{c(3) - c(1)}{2}) + E] \quad (27)$$

The concentration near the bed is determined, assuming the concentration gradient in the layer $0 < z < a$ being equal to the gradient at height $z = a$ (linear extrapolation).

$$(\frac{\partial c}{\partial z})_{z \le a} = -\frac{c(a).w}{\bar{\varepsilon}_s} \quad (28)$$

The concentration at the bed level is consequently:

$$c_{z=0} = c_a + \frac{c_a . w . a}{\bar{\varepsilon}_s} = c_a . (1 + \frac{a . w}{\bar{\varepsilon}_s}) \tag{29}$$

In numerical approximations:

$$c(1) = c(2) + \Delta h (\frac{\partial c}{\partial z})_{z=2} = c(2) + \Delta h (-\frac{c(3) - c(2)}{\Delta h}) \tag{30}$$

$$= 2.c(2) - c(3)$$

Substituted in ***equation (27)***:

$$c(2)_{t=t+\Delta t} = c(2)_{t=t} + \frac{\Delta t}{\Delta h}[(0.8(\bar{\varepsilon}_s \frac{c(3) - c(2)}{\Delta h}) + w(c(3) - c(2)) + E] \tag{31}$$

Similarly, the concentration at the water surface is determined: the vertical sediment transport for i=m and i=m+1 are defined according to the ***equations (18) and (19)***, whereas the transport for i=m+1 is zero, because no sediment transport will take place through the water surface.

The fluctuation of the concentration in i=m+1 follows from:

$$c(m+1)_{t=t+\Delta t} = c(m+1)_{t=t} + \frac{\Delta t}{\Delta h}[\bar{\varepsilon}_s (\frac{c(m) - c(m+1)}{\Delta h}) - w(\frac{c(m+1) + c(m)}{2})] \tag{32}$$

The sediment transport is obtained from the concentration distribution and the velocity. The horizontal sediment transport is determined, according to the following equation:

$$S_x(t) = \sum_{i=2}^{m+1} c(i) v(i) \Delta h \tag{33}$$

By schematizing the equations numerically, certain errors are introduced in the calculation. These errors are examined in ***appendix 4.1.***

§ 4.4 Stability of the numerical scheme

The stability of the numerical scheme can be checked by applying the Von Neumann theory. The complete derivation of the stability analysis are in ***appendix 4.3***. The concentration at level j at time t=0 is written as a Fourier series; each term is considered separately:

$$c^0(j) = c_0 e^{ik\Delta z} = c_0 e^{ij\xi} \tag{34}$$

$$\xi = k\Delta z = \frac{2\pi\, dz}{L} \tag{35}$$

Now the concentration $c^1(j)$ (at time t=1) corresponding with ***equation (22)*** is written as a function of $c^0(j)$. This relation is converted to a form like

$$c^1(j) = \rho \,.\, c^0(j) \tag{36}$$

wherein ρ is the amplification factor. This way, the concentration for time step t= n.t can be written as:

$$c^n(j) = \rho^n c^0(j) \tag{37}$$

The demand of the stability runs:

$$|\rho| \leq 1 \text{ for } 0 \leq \xi \leq \pi \tag{38}$$

Elaboration of ρ leads to the stability criterion:

$$\frac{w^2 \Delta t^2}{\Delta h^2} \leq \frac{\bar{\varepsilon}_s dt}{\Delta h^2} \leq 0.5 \tag{39}$$

§ 4.5 Programme Structure Diagram

The programme structure diagram gives information about the structure of the programme, therefore, changes or improvements can be assembled properly.

```
read input
calculation of  v*, ε, dh, β, δ
t = 1
calculation concentration profile with c(2)
determination average concentration
computation sediment transport
appoint and write velocity profile
DO WHILE t < t (end)
    t = t + dt
    calculation v* with v(t)
    computation new concentration profile
    computation new δ
    DO EVERY HALF HOUR
        write new concentration and velocity
        profiles to arrays
        determine new average concentration
    DO EVERY 20 MINUTES
        write t,v(t),e(t),ε1,ε2,v*,cgem to a file
        computation s
        write s
        DO WHILE t < t(period)
            write sflood,sebb
            sfloodtot = sfloodtot + sflood
            sebbtot = sebbtot + sebb
        check stability
        ε1 = ε2
        new concentration = old concentration
write sebbtot,sfloodtot
```

Chapter 5 The programme in operation

Introduction

The computer programme, which calculates the vertical sediment distribution, can be used after the input is determined. The programme is extended with plot utilities in order to produce graphs of the concentrations versus time, and the concentration and velocity distribution over the vertical. As stated earlier, the location III-B is chosen for investigation, therefore the values of the parameters will be adapted for location III-B. First, the programme is run unaltered, yet later on some changes are made to improve the fits of the concentrations.

§ 5.1 Influence of the input parameters on the concentration distribution

The values of the parameters such as the fall velocity, the shear stress velocity and the Chézy coefficient, cannot be determined exactly. Different formulae give different results within a certain range (see ***appendix 5.1***). The values can be changed within this range in order to get a better fit of the calculated concentrations to the measured concentration.

§ 5.1.1 The input of the programme

Introduction

The programme needs several parameters as input in order to calculate the concentration distribution over the vertical. The parameters depend on the hydraulic conditions and on the characteristics of the suspended material.

The needed input parameters are displayed in ***table 5.1***. The elaborate derivation of the values of the input parameters are described in ***appendix 5.1***.

The range of the fall velocity is rather large. The range of the critical shear stress velocity is smaller, but a change of the value of the critical shear stress velocity has a large impact on the concentration distribution. The rate of the entrainment factor depends largely on the critical shear stress velocity. The entrainment factor is responsible for the exchange of the grains between the bed and the fluid, thus the amount of suspended material depends on the entrainment factor. Without supply of suspended sediment from the bed, there are no grains that can be transported upwards in the vertical.
The initial input of the programme is written in ***table 5.2***.

Table 5.1

parameter	description	unity
m	number of layers	
h	water depth	m
w	fall velocity	m/s
v_0	initial current velocity	m/s
$v_{*,cr}$	critical shear stress velocity	m/s
D_{50}	grain size	m
dt	time step	s
T_{end}	finishing time	s
Per	tidal period	s
cv(2)	initial value of concentration	g/m^3
κ	Von Karman constant	
ϵ	diffusion coefficient	
nt	number of input of velocities	
step	time interval between input velocities	s
table	table of velocities	m/s

Table 5.2

param.	value	unity	param	value	unity
m	7	[m]	Per	45120	[m]
h	6.9	[m]	cv(2)	2030	[g/m^3]
w	0.0035	[m/s]	kappa	0.4	[]
v_0	0.9958	[m/s]	α	0.06	[]
$v_{*,cr}$	0.012	[m/s]	nt	60	[s]
D_{50}	70.10^{-6}	[m]	step	752	[]
dt	3	[s]	table		[m/s]
T_{end}	45120	[s]			

The variables investigated on their influence on the calculation are:

-1 the Chézy coefficient, influencing the magnitude of the shear stress velocity, according to formula:

$$v_* = \frac{v}{\theta}, \qquad \theta = \frac{C}{\sqrt{g}}$$

The factor Θ was 20 m^{½}/s in the original programme, thus the Chézy coefficient was taken 62.64 m^{½}/s.

-2 the fall velocity

-3 the critical shear stress velocity

-4 the factor α in the diffusion coefficient

§ 5.1.2 Discussion of the impact of the parameters

Introduction

The parameters, mentioned in the previous section, were changed one by one in order to investigate the influence of the individual parameters. The results are shown in the ***figures 5.1.2.1 up to 5.1.2.6. Table 5.3*** shows the values of the input parameters that correspond to the figures.

Table 5.3

figure	w [m/s]	v*,cr [m/s]	alpha []	theta []
5.1.2.1	0.005	0.012	0.05	20
5.1.2.2	0.005	0.012	0.05	30
5.1.2.3	0.003	0.012	0.05	30
5.1.2.4	0.005	0.01	0.05	30
5.1.2.5	0.005	0.01	0.08	30
5.1.2.6	0.005	0.01	0.03	30

The figures show the measured concentrations at the water surface (csurf) and at the bed (cbot), represented by the dashed lines, and the calculated concentrations cv(i) versus time. The starting time is 8:30 hrs, because the velocity registrations started at that time.

Here, the surface concentration must in theory lie between the lines of cv(7) and cv(8) and the bottom concentration between cv(2) and cv(3). This goal is not yet achieved, but the following experiments were performed in order to get a better view on the influences of the parameters. The upper line represents the concentration at layer 2 (cv(2)) and the lines below that one represent the layers with a higher rank, in rising order.

The Chézy coefficient

The Chézy coefficient in case of ***figure 5.1.2.2*** was changed to 94 $m^{½}/s$, which brings on a Θ of 30. Compared to ***figure 5.1.2.1***, the concentrations are much lower and come closer to the surface and bed concentrations declared in the figures as respectively csurf and cbot. This value of the Chézy coefficient is also used in the following runs, because the runs of the flow model of the area indicate smoothness of the bed, therefore using a high Chézy coefficient gives good results. When the bed is smoother, the turbulence of the water near the bed diminishes, and for this reason the mixing (diffusion) decreases and so does the sediment concentration in the water.

The fall velocity

In case of ***figure 5.1.2.3***, the fall velocity is converted to 0.0025 m/s. Both concentrations are higher, even near slack water, where the velocity is close to zero. When the velocities are low, the concentrations are generally too low and the difference between the surface and the bottom concentration is too small. This indicates that the mixing of the sediment is reproduced too strongly in the calculation. This can be solved by decreasing the diffusion coefficient.
The decrease of the fall velocity causes the particles not to settle, but rather, to stay in suspension. Consequently, the concentration is higher. Following from ***equation (2)***, further on in this section, the concentration gradient increases as the fall velocity increases, which can be observed in the graph of ***figure 5.1.2.3***.

The critical shear stress velocity

The reduction of the critical shear stress velocity (***figure 5.1.2.4***) results in high concentrations as both at the bed and at the water surface. During the fluctuations of the velocity over the tidal cycle, the bed material is brought in suspension at a lower velocity than is the case in ***figure 5.1.2.2***. The entrainment factor is a function of the critical shear stress velocity. When the critical shear stress velocity is lower, more sediment is picked up from the bed (under lower flow velocity conditions, thus over a longer period within the tidal period). This is represented by an increased entrainment factor, which results in increased concentrations.

The diffusion coefficient

The change of the constant α in the diffusion coefficient influences the mixing of the suspended material over the vertical. This is displayed in the ***figures 5.1.2.5 and 5.1.2.6***. As α increases, the mixing is stronger and more sediment is transported upwards, thus the concentrations at the surface and the bed come closer. The surface concentration is higher than in case of ***figure 5.1.2.3***. In case of a reduced α, less upward sediment transport in the vertical occurs, the surface concentration therefore being lower. The measured surface concentrations are higher, especially at slack water.

During the first time step, the concentration is calculated according to the equilibrium profile and further on, according to the continuity equations. The effect of the first time step lasts for about one and a half hour only. For this reason, its effect is limited. However, the concentration distribution on t = 0 gives an indication of the choice of the parameters.
According to the following formula,

$$c(i) = c(2) \cdot e^{\frac{-w.dh.(i-1.5)}{\varepsilon_s}} \qquad (2)$$

the concentration distribution depends on the factor:

$$\frac{w.dh}{\varepsilon_s}$$

The magnitude of the fall velocity, the diffusion coefficient and their ratio influences the magnitude of the range and the concentrations. If this factor is larger, the range will be larger, but the concentration decreases as well. Other influences on the results are the entrainment factor and the Chézy coefficient via the shear stress velocity in the diffusion coefficient.

§ 5.2 Mechanism of the continuity equation

The different parts of the continuity equation are plotted against time in order to investigate the mechanism of the sediment distribution in the vertical. See ***figures 5.2.1 and 5.2.2*** for respectively layer j=2 and layer j=5.

For j=2 and j=5, the fall velocity and the diffusion coefficient part of the following equations and the summation of both parts, are divided by the concentration in the belonging layers. For j=2, the same is performed for the entrainment factor.
In this way, the relative influence of the different parts on the alteration of the concentration in time is displayed, whereas the relative value of the concentration of the previous time step is 1.

For j=2:

$$c(2)_{t=t+dt} = c(2)_{t=t} + \frac{dt}{dh}\left[(0.8\,\overline{\varepsilon}_s \frac{c(3)-c(2)}{dh}) + w(c(3)-c(2)) + E'\right]$$

For j=5:

$$c(5)_{t=t+dt} = c(5)_{t=t} + \frac{dt}{dh}\left[\overline{\varepsilon}_s (\frac{c(4)-2c(5)+c(6)}{dh}) + w(\frac{c(6)-c(4)}{2})\right]$$

For j=2, the line types in ***figure 5.2.1*** represent (from left to right): the diffusion part, the fall velocity part, the entrainment factor part and the resultant of those parts of the equation. Near the bed, the entrainment factor has a relatively large influence on the concentration and results in an increase of the concentration, whereas the fall velocity and diffusion part of the equation tend to decrease the concentration. The curves fluctuate considerably.

The concentration of the previous time step is still the most important part of the formula, but the other parts influence the increase or decrease of the concentration in time. This effect is amplified every time step within the concentration of the previous time step. (Like the amplification factor of ***section 4.4***).

The first and second derivatives in z-direction of the concentration are of a comparable magnitude, because:

$$\frac{d^2c}{dh^2}_{(i=2)} = \frac{\frac{dc}{dz}}{dz} = \frac{\frac{c(3)-c(2)}{dh}}{dh} = \frac{c(3)-c(2)}{dh^2} \qquad (6)$$

and dh $\approx$ 1 m. Since the value of the ratio ϵ_s/w is generally 4 to 5, depending on the magnitude of the velocity via the shear stress velocity in the diffusion coefficient, the diffusion part is generally larger than the fall velocity part.

For j=5, the fall velocity part works in the opposite direction of the diffusion part. The curves are smoother than for j=2. For j=5, the first derivative is significantly larger than the second derivative, whereas the fall velocity is smaller than the diffusion coefficient. These opposing qualities result in fall velocity and diffusion parts of comparable magnitude.

When the tide turns (in ***figures 5.2.1 and 5.2.2*** at count 4 and 16, respectively at 10:30 hrs and 16:00 hrs) both parts have a relatively large influence on both the alteration of the concentration, and on the resultant, which changes fast from a

negative maximum value to a positive maximum value. Thus, during slack water, the significant changes in the concentration gradient in time take place. This period of time is the most important for developing a good simulation of the measured concentrations. During the decrease of the concentration, the diffusion part slowly diminishes to approximately zero, as the fall velocity part falls back to a constant value of 0.002.

The result of both occurring phenomena under decreasing velocity is that the effect of the diffusion part is gradually dominated by the fall velocity. When the velocity increases, the reverse mechanism occurs in a shorter time period.

General shape of the curves:

The peaks in all parts of the formulae occur when the concentration is increasing after slack water.
The curves of j=5 are smoother than the curves of j=2, probably because the system of uplifting and settlement of the particles is subdued higher up in the vertical. The fall velocity part dominates when the velocities are low, allowing the sediment to settle. When the velocities are high, the diffusion coefficient part dominates, uplifting the particles further in the vertical.

§ 5.3 Alteration of the programme

In general, the results of the programme are partly satisfactory. The concentrations during times of low velocities are usually too low. Some alterations are implied in order to improve the results of the programme.

The alterations are:

-1 The depth is changed from constant to time dependable according to the tidal curve.
-2 The Chézy coefficient is altered as well, as it is a function of the depth.
-3 The impact of ripples on the Chézy coefficient is implemented in the programme.
-4 The entrainment factor is determined in the same manner as is performed in Prins [1977], but using the measured concentrations at the bed for c_a.
-5 The presence of wash load is simulated by using a reduced fall velocity when the flow velocity is low.

The elaboration of these alterations and their results are discussed in the following sections.

§ 5.4 Variable water depth

The depth is assumed to be constant, but as the water level changes between 5 m to 9 m approximately, the water level being a function of the time will be given as input. The fluctuation of the water level does not have a large impact on the concentration, but the horizontal sediment transport follows from the equation:

$$S_x(t) = \sum_{i=1}^{m} \tfrac{1}{4}\,[\,c(i) + c(i+1)\,]\,[\,v(i) + v(i+1)\,]\,dh \qquad (7)$$

thus the product of the concentration and the velocity are integrated over the depth. Therefore, the depth influences the horizontal sediment transport.

The depth in III-B is determined from the tidal registrations from the Oil Jetty. Then the layer thickness is determined by dh = h(t)/m, wherein m is the amount of layers. The continuity equation (***formula (5) in § 4.2***) still holds. The volume of the water in the unity block remains constant, because of the continuity equation of the water. (Being an ideal fluid, water is incompressible.) Therefore, the width of a unity block (***see figure 4.3.1***) also fluctuates in time. In this way, the volume of the unity block stays the same, independent of time.

§ 5.5 The Chézy coefficient as function of the depth

The Chézy coefficient is made depended of the depth according to the following formula:

$$C = 18 \log\left(\frac{12\,h(t)}{r}\right) \qquad (8)$$

The bottom roughness r in ***formula (8)*** is chosen from the values of ***table 5.1.3***. Following from the high Reynolds numbers that are valid under the circumstances of III-B, the Chézy coefficient should theoretically be calculated by the formula:

$$C = 18 \log\left(\frac{12\,h(t)}{r + \frac{\delta}{3.5}}\right), \quad \delta = \frac{11.6\,\nu}{v_*} \qquad (9)$$

This results in the Chézy coefficient being dependent of the shear stress velocity, which is a function of the Chézy coefficient. Therefore, an iteration process must take place, which amplifies the calculation time. Furtheron, the change in magnitude of the Chézy coefficient is small: 0.8 % up to 4 %, the Chézy coefficient being about 95 $m^{0.5}/s$. In order to avoid an unneccesary long calculation time, the Chézy coefficient is calculated occording to formula (8).

The dependence of the concentration of the depth is small: no significant changes have taken place. The distribution of the concentration over the vertical decreases, as can be seen in ***figures 5.3.1 and 5.3.2***. This is the result of an increasing

Chézy coefficient.
Figure 5.3.1 shows the concentrations, determined by a calculation with constant depth, whereas ***figure 5.3.2*** is a result of a calculation with variable depth and Chézy coefficient. According to ***equation (10)***:

$$c(i) = c(2) \cdot e^{\frac{-w.dh.(i-1.5)}{\varepsilon_s}} \qquad (10)$$

The distribution of the concentration over the vertical depends on:

$$\frac{w\ dh}{\varepsilon_s} \qquad (11)$$

As the diffusion coefficient is a function of the shear stress velocity, the shape of the concentration vertical depends on the relation w/(v*). This relation is also responsible for the erosion rate in time as seen in ***equation (20) in section 4.3***.

The influence of the layer thickness dh in the numerator is eliminated, because the depth in the diffusion coefficient of the denominator equals h(t)=m*dh(t). The Chézy coefficient, applied while calculating the shear stress velocity, is still a function of h(t).
The amount of layers (m) influences the concentration distribution over the vertical, but this amount is not changed, because a calculation with more layers will give a more accurate result, but will introduce a much smaller time step dt. This follows from the stability demands. If the water depth is divided in a large number of layers, the influence of the amount of layers on the accuracy is low. Yet, the applied amount of layers is limited because of the stability demand. The time step which has been used is 3 seconds, which already introduces a fairly long calculation time over one tidal cycle, when this model is implemented in a sediment transport model for the whole area.

§ 5.6 The Chézy coefficient including ripples

The Chézy coefficient is assumed to be fairly high, indicating a plane bed situation, which also follows from the results with the flow model of the area. The presence of ripples is not included in the current version of the programme, contrary to van Kooten [1974] and Prins [1977] who did take ripples into account when determining the entrainment factor.

In this section, an estimation is made of the influence of ripples, which maybe present at the bed at some period of the tidal movement. The calculations are not assumed to be correct, but will merely give an indication. As it happens, the formulae are derived from flume experiments under steady flow conditions. However, as a result of the tidal movement, the flow velocity is constantly changing. These formulae are nevertheless applied in this situation, assuming that the flow is steady per time step. This is done in order to find a possible solution for the high concentration during slack water.

The fine material and the high velocities lead to plain bed situations, but when the velocity diminishes near slack water, ripples and dunes can be formed. These ripples and dunes cause an increased roughness of the bed, that corresponds with lower Chézy coefficients, which influences the concentration. When the flow moves over a rough bed, the turbulent movement encourages diffusion. The sediment can therefore easily be moved up in the vertical. The fact that it takes some time for the bed to adjust to the changed flow conditions is neglected. Therefore, the dimensions of the ripples are overestimated.

The determination of the Chézy coefficient via roughness factors from curves of Lovera-Kennedy and Alam-Kennedy cannot be performed in the way this was done in van Kooten [1974]. The magnitude of the values at the axes in case of III-B exceed the maximum values, caused by the combination of a large depth and fine grains.

In van Rijn [1990], a different method to determine the existence of ripples and dunes is presented. This method is described in ***appendix 5.2***.

The bed roughness resulting from the ripples can be calculated from the heights and lengths of the ripples. This bed roughness must be added to the grain roughness, but the latter can be neglected when comparing to the bed form roughness.

The Chézy coefficient is determined according to the formula of White-Colebrook. As the velocity changes rapidly as a result of the tide, the ripples are obviously not able to reach an equilibrium form. Thus, the ripple sizes are not expected to reach their maximum size.
The creation of ripples can also be induced by waves, but since the bed material partly exists of mud, the sediment concentrations, generated by wave action, dramatically reduce van Rijn [1985]. Another reason for not taking wave action into account is that in the rest of the programme, wave action is also ignored: for this reason, it is inconsistent to take waves into account here.

Since the limits between the ripples and the plane bed are drawn sharply, a discontinuity occurs in the Chézy coefficient. The meaning of this exercise was to investigate the influence of ripples on the concentration, especially for the concentrations during low velocities, which are generally too low, except if the input is such that the concentrations during ebb and flood are too high.

It was assumed that when diminishing the Chézy coefficient for low velocities, the shear stress velocity would increase. In this way, the period wherein the critical shear stress exceeds the shear stress velocity is smaller, thus the concentration will not diminish so much.

The programme was altered in such a way that ripples were taken into account in the calculation of the Chézy coefficient. The results are shown in ***figure 5.6.1***. The concentrations near slack water were not significantly higher than during calculations without ripples, and the difference in concentration between the bed and the surface became smaller. As a result of the increased bed roughness, the turbulence of the water increases and the mixing of the sediment over the vertical enhances. A discontinuity in the concentration development in time occurs, because of the discontinuity in the calculation of the Chézy coefficient.

Although the concentrations increased slightly during the slack water period, the results were not improved dramatically. Combined with the discontinuity and the application of the formulae under non-equilibrium conditions, it was decided not to take the possible existence of ripples into account.

§ 5.7 Determination of the entrainment factor

The entrainment factor in the reports of Prins [1977] and van Kooten [1974] is determined by generation of velocities, matching shear stress velocities and concentrations, following from the sediment transport curves of Colby. The bed load sediment transport is considered negligible compared to the suspended sediment transport, because of the fine material that is present in this area. The entrainment factor, calculated for the equilibrium state, $E=0.8*c_a*w$, is plotted against the factor:

$$[(\frac{v_*}{v_{*,cr}})^2-1] \qquad (12)$$

on double logarithmic scale. From this curve, the relation for the entrainment factor is derived.

The entrainment factor in case of position III-B is determined in the same manner as described above. The concentration, measured near the bed during the measuring campaign, is used as concentration c_a. The shear stress velocity is calculated with the measured velocity and the Chézy coefficient as described in ***section 5.5***.

Figure 5.7.1 shows the simulation of the concentration, which fits rather well. The distribution over the vertical is well schematized, but the concentrations under low velocity conditions are still too low.

The use of this entrainment factor is an improvement of the programme. The entrainment factor gives the best results with the input variables that are used for the determination of the entrainment factor. Other sets of input variables give acceptable results, but are not optimal.

The entrainment factor was determined for coarser material than is present in Haldia. This introduces different Chézy coefficients which results in different shear stress velocities. The critical shear stress velocity depends on the grain size as well. These are the variables, responsible for the slope of the function for the entrainment factor.
The entrainment factor is determined by van Kooten [1974], using curves that give sediment transport as a function of the depth, the velocity, and the grain size of the bed material. These curves were determined by experiments in flumes, with a depth of 0.3 m and 3 m. The results were extrapolated to a depth of 10 m. The curves only exist for grain sizes, larger than 100 μm. The material present in III-B and I-A is smaller. The grain size has influence on the Chézy coefficient and the critical shear stress velocity.

The depth is responsible for the value of the angle of slope of the entrainment factor, which is shown in ***figure 5.7.2***. The twist in the curve results from the change of the Chézy coefficient, which is caused by the ripples that are present at low velocities. When the velocity increases, the ripples disappear and the Chézy coefficient increases.

Both depth and grain size influence the magnitude of the entrainment factor at which the curve twists, on which the relation $v_*/v_{*_{cr}}$ does not have much influence. The specific data of the Hooghly River provides in a larger depth, smaller grain sizes and higher velocities than the combination of values for which the entrainment factor is determined. Therefore, the entrainment factor of van Kooten [1974] does not provide the optimal results for the simulation of the vertical sediment transport in III-B.

§ 5.8 The fall velocity

In case of an acceptable simulation of the concentration distribution over the vertical in time, the concentration near slack water is always too low. This is in contrast to the measured concentrations at the surface and the bed.

First, it was tried to model the effect of segregation of the grains over the vertical as a result of different fall velocities. Smaller particles, which have a lower fall velocity, do not settle as fast as particles that are heavier. In the upper part of the vertical, there will be smaller particles present than in the lower part of the vertical.

The programme was modified by calculating with a lower fall velocity for the upper half of the vertical, than was done for the lower half. The results were unsatisfactory and consequently, this alteration was eliminated from the programme.

Another plausible explanation is the presence of wash load. The material at the bed is very fine and a considerable amount of mud is present. The mud in suspension will not settle over the short period of slack water, when the velocities

are low. Therefore, the mud stays in suspension, causing the minimum concentrations to be relatively high.

In order to simulate this mechanism, two fall velocities are used in the programme: the fall velocity belonging to the grain sizes according to the bottom samples, and a fall velocity having the magnitude of mud particles. The latter fall velocity is implemented in times of low flow velocities, when the predicted concentrations according to the usual procedure is low. The calculated concentrations around slack water are now higher. This way of simulating the wash load introduces a discontinuity in the concentrations.

The result is shown in ***figure 5.8.1***. The concentrations during slack water are considerably higher than in the figures of previous sections, but the concentration distribution is not sufficient enough. This way of schematizing the fall velocity combined with the entrainment factor of ***section 5.7*** will result in better fitting curves.

Another way of dealing with wash load is to subtract the lowest measured surface concentration (at count 16) from the all measured concentrations. Accordingly, this set of data needs to be fitted by the programme. The remaining lowest concentration near the first slack water (count 4) is significantly higher than zero. This is, however, not properly indicated by the programme. After running the programme, the value of the measured concentration at count 16 needs to be added to the predicted concentrations.

It must be noted that simulating the concentration near slack water accurately is of secondary importance; the amount of horizontal sediment transport during slack water is relatively small due to low concentrations as well as low velocities.

§ 5.9 Conclusions

The measured concentrations were not properly simulated by the original programme, as the predicted concentrations are too low when low velocities occur during phases of the tidal period.

When using a depth variable in time instead of a constant depth (as in the original programme), the horizontal sediment transport increases. The influence on the concentration distribution is moderate.

As the Chézy coefficient is made depth dependable, the diffusion coefficient is influenced via the shear stress velocity.

The problem of the decrease of the concentration to approximately zero under low velocity conditions cannot be solved by taking ripples into account during the determination of the Chézy coefficient. The possible existence of ripples is further ignored.

When a function to represent the entrainment factor is fitted with the measured concentrations, a better fit of the measured concentrations can be obtained.
The conditions, under which the original entrainment factor was determined, did not correspond to the conditions in Haldia. The material present in Haldia is smaller than the material used in the calculation of Prins [1977] and van Kooten [1974]. Further on, the data in Prins [1977] is derived via curves of Colby, following from flume experiments under steady flow conditions, for depths of 0.3 m and 3 m extrapolated by Prins [1977] to 10 m.
By using the measured concentrations, the method to determine the entrainment factor is applied more specifically on the situation of Haldia, the different input variables are therefore better geared to one another. This results in a better fit, which shows the importance of the relation between the various input variables.

The measured concentration around slack water is fairly high. This can be explained by the existence of wash load. The effect of wash load can be simulated in the model by inserting a fall velocity of mud into the programme when the velocity is low. The concentrations under low velocity conditions can now be approached in a better way.

The equation dealing with the shape of the concentration over the vertical was altered according to suggested formulae for the concentration distribution and matching diffusion coefficient by Bhattacharya, Rouse/Einstein and van Rijn in van der Velden [1989]. These formulae did not yield better results regarding the measured concentrations and the high concentrations during slack water. They merely introduced complications because of their definition of the diffusion coefficient, which results in concentrations of infinite magnitude near the bed. The curve of the concentrations plotted against time did not fit in a better way than was the case with the original diffusion coefficient and matching concentration distribution. Therefore, they were not altered.

Summary

For shipping to take place from the Bay of Bengal to Calcutta, a deepening of Haldia channel across Balari Bar is required. Because of the complicated system of ebb and flood channels and the large amounts of sediment that are transported through the system, a computer programme needs to be developed in order to predict the spoil volume of the dredging activity required. A computer programme needs data for calibration. This data is obtained by carrying out a measuring campaign.

First it is investigated what kind of information is necessary for this calculation. Next, the measuring instruments are chosen. A general working method was developed after evaluating the previous campaign. Next, a time schedule was set up.

During the campaign the flow velocity was measured, water and soil samples were taken, and cross lines were sailed in order to measure water depths. Flow lines were traced by following floats and water level registrations over a long period were obtained at the semaphores. Afterwards, the water samples were filtrated and the soil samples were sieved in Holland.

The data that was obtained during the measuring campaign is discussed in ***chapter 2***. The variety in magnitude of the amplitude of the velocity in I-A over the spring-neap period is studied by observing the output of the velocity meter. The influence of the depth of the velocity meter on the magnitude of the velocity is discussed, and the velocities at the different locations are compared to each other; taking into account the neap spring variation. The global locations of ebb and flood channels are determined by looking at the amplitudes of the velocity during ebb and flood. Further on, the water level registrations, the concentration measurements, the soil samples and water density measurements are discussed.

In ***chapter 3***, a Fourier series is fitted to the tidal movement according to the method of harmonic analysis. The length of the observation interval and the time step are determined, corresponding to the theory of spectrum analysis. The data was obtained from the Oil Jetty, an Indian water level registration station in the area of interest.

To sort out the significant angular frequencies in this particular observation interval, a spectrum analysis was applied to the dominant angular frequency ranges. These ranges were derived from a table of angular frequencies of frequent occurrence.

The spectrum analysis works as follows:
The angular frequency ranges are split up in angular frequencies of equal distance. These angular frequencies are subjected to a Fourier analysis, which results in the belonging amplitudes being given as output. The most significant angular frequencies are selected from graphs on which the amplitudes are plotted against the angular frequencies. These angular frequencies are used to simulate the tidal movement. The result of subtracting the fit of one angular frequency range from the signal is investigated to find out the influence the different angular frequency ranges on the tide. The significant harmonic and shallow water components are derived from the

results of the spectrum analysis. These angular frequencies are used for a harmonic analysis.
The impact of the components on a single tidal wave are studied. The obtained amplitudes from the harmonic components are compared to the predicted components of the Admiralty Tide Tables.

In ***chapter 4***, the theory of the programme that determines the vertical concentration distribution of the suspended sediment under non-permanent flow conditions is discussed. After assuming certain profiles for the velocity and the concentration, the latter is determined as a function of the time following from a continuity equation for the sediment. The change in concentration during one time step is determined from the nett vertical sediment transport. This transport exists of a fall velocity part and a diffusion part. The vertical sediment transport near the bed also exists of an entrainment factor. The equations were numerically approached and the stability demands were checked.

The input parameters are determined in ***chapter 5***. Next, the input parameters are varied in order to determine the impact of the parameters on the calculation. The influences of the parts of which the continuity equation exists are examined. Some alterations are implemented in the programme such as a variable water depth instead of the constant water depth of the original programme, and a Chézy coefficient that is depth dependent. The predicted concentrations near slack water are generally too low, compared to the measured values. In an attempt to improve this, the influence of ripples on the Chézy coefficient is implemented in the programme. The results were not satisfactory. The entrainment factor was determined using the measured concentrations, causing them to match better.
The wash load, that causes high concentrations around slack water, is simulated by implementing a low fall velocity in the programme in case of low velocities. This results in significantly higher concentrations near slack water.

Recommendations

-1 The shape of the velocity profile cannot be determined by the measurements, because the registrations were only performed at one depth at the time except for location I-A. However, it is assumed that the pontoon has influenced the velocity meter registrations. Moreover, the difference in depth between both meters was small, as the meters were uplifted by the flow. A profile can therefore not be determined. For this reason, the velocity profile is assumed to be represented by the logarithmic equation of Keulegan (***equation (2), section 4.2***).
A new way to keep the velocity meter at a certain depth must be developed in order to avoid uplifting by the flow. The shape of the velocity profile can be determined by measuring the velocity at several depths at one location, at approximately the same moment in time.

-2 The horizontal sediment transport is not investigated, because the model, described in ***chapter 4***, gives information only about the sediment distribution at one location. For this reason, the horizontal transport can only be determined per meter width. As the amount of erosion or accretion is usually determined from differences is depth soundings at different moments in time, the determined horizontal sediment transport cannot be verified, because the area of the location has not been defined.

-3 The concentration distribution is investigated only at location III-B, due to lack of time. It is recommended to apply the programme to data of the other locations, at which concentration measurements took place as well.

-4 The depth at which the water samples are taken was roughly estimated, although the concentration gradient is fairly high near the bed. Therefore, the shape of the concentration distribution can not be determined with great accuracy. A number of two measurings in the vertical is too small to determine the shape of the concentration profile anyhow. It is recommended to determine the depth were the water sample is taken more accurately. A number of three samples per vertical would be better, but it takes a long time to process the samples then.

-5 A comparison between the horizontal sediment transport, determined by the product of the mean depth value of the concentration, and the velocity and the transport following from ***equation (32)*** in ***section 4.3***, will give information about the diminished accuracy, using the first manner of

determining the horizontal sediment transport. The transport, determined from the mean values, will reduce the calculation time of the sediment transport model of the area.

-6 The time step and layer thickness can be varied, taking the stability demands into account. By diminishing both values, the accuracy will increase (for low values of both parameters). However, the calculation time will increase. The decrease of the layer thickness is limited, because this action increases the stability factor. For both reasons, the time step that is determined in ***appendix 5.1*** is used in every calculation.

Literature

Admiralty Tide Tables and tidal stream tables volume 2, 1991
The hydrographer of the navy
N.P.202-91

Allersma, Ir.E. and de Groot, dr.A.J., 1975
Article Intermediair
11e jaargang 43, 24 oktober 1975
Transportverschijnselen in estuaria
Emmeloord, Groningen

Cheng, R.T.
Coastal and Estuarine Studies
Residual Currents and Long-term Transport
ISBN 0-387-97376-1
ISBN 3-540-97376-1

Dyer, K.R., 1986
Coastal and Estuarine Sediment Dynamics
Institute of Oceanographic Sciences, Bidston, UK
John Wiley and sons

Euromech 177 Colloquum, (June) 1989
Mathematical modelling of sediment transport and morphology
Abstracts of participants
Delft, The Netherlands

Eysink, W.D. and Vermaas, H., (June) 1983
Computational methods to estimate the sedimentation in dredged channels and harbour basins in estuarine environments
publication no. 307

Graf, W.F., 1971
Hydraulics of sediment transport
Mc-Graw-Hill

Hooghly fairway development project, (november) 1990
Work method statement
Part I, phase 1 and 2

Kalkwijk, dr.ir. J.P.Th., (september) 1976
Analyse van Getijden, naar het college "Getijden" (b75)
Delft, tweede herdruk juni 1983

Kooten, F. van, (november) 1974
aspecten van het uitwisselingsproces van zwevend zand met de bodem in een open waterloop
Afstudeerverslag TH Delft, Civiele Techniek

Network sedimentation model, (May) 1986
description of program package
SEFLOW
Delft Hydraulics Laboratorium

Nortier, ir. I.W. and Velde, ir. H. van der, (januari) 1961
Hydraulica voor waterbouwkundigen
Technische uitgeverij H.Stam N.V.
Haarlem

Norušis, Marija J.,/SPSS Inc.
SPSS/PC+ Statistics™ 4.0
for the IBM PC/XT/AT and PS/2
ISBN 0-923967-12-5

Prins, J.P.G., (januari) 1977
Verticale concentratieverdelingen van zwevend sediment bij niet-permanente stroming
Afstudeerverslag TH Delft, Civiele Techniek

Raalte, G. van, (January) 1988
Deskstudy dredging
Report on a morphological deskstudy of the Hooghly River Estuary

Raudkivi, A.J., (January) 1965
Loose boundary hydraulics
Pergamon Press
Auckland, New Zealand

Reus, J.H. de, (april) 1979
sedimenttransport
berekening van de sedimentconcentratie in de vertikaal bij niet-permanente stroming
speurwerkverslag S 151 deel II
Waterloopkundig Laboratorium

Sand, Stig E., (January) 1986
Stochastic processes: Practical Computation of Spectra
Danish Hydraulic Institute

Svasek, ingenieursbureau, (April) 1988
The development of the estuary in the 20th century
Project 770

Velden, Ir. E.T.J.M. van der, (February), 1989
Coastal Engineering, Volume II
f7 Morfologie van kusten en estuaria
TU Delft The Netherlands
602010

Voogt, Leo C. van Rijn, Leo C. and van den Berg, Jan H.
Article Bagt 910051
Sediment transport of fine sands at high velocities

Wang, Z.B., 1989
Mathematical Modelling of Morphological Processes in Estuaries
proefschrift TU Delft, Civiele Techniek